ÉCOLE POLYTECHNIQUE FÉDÉRALE DE LAUSANNE

MATHICSE

Mathematics Institute of Computational Science and Engineering

School of Basic Sciences - Section of Mathematics

MATHICSE Technical Report

Nr. 14.2013

April 2013

Interface control domain decomposition (ICDD) methods for coupled diffusion and advection-diffusion problems

M. Discacciati, P. Gervasio, A. Quarteroni

http://mathicse.epfl.ch

Phone: +41 21 69 37648

Address:
EPFL - SB - MATHICSE (Bâtiment MA)
Station 8 - CH-1015 - Lausanne - Switzerland

Fax: +41 21 69 32545

21 April 2013. Submitted to:*Int. J. Numer. Meth. Fluids*

Interface Control Domain Decomposition (ICDD) Methods for Coupled Diffusion and Advection-Diffusion Problems

Marco Discacciati[1], Paola Gervasio[2*] and Alfio Quarteroni[3]

[1] *Laboratori de Càlcul Numèric (LaCàN), Escola i Tècnica Superior d'Enginyers de Camins, Canals i Ports de Barcelona (ETSECCPB), Universitat Politècnica de Catalunya (UPC BarcelonaTech), Campus Nord UPC - C2, E-08034 Barcelona, Spain.*
[2] *DICATAM, Università di Brescia, via Branze 38, I-25123 Brescia, Italy.*
[3] *MOX, Politecnico di Milano, P.zza Leonardo da Vinci 32, I-20133 Milano, Italy and MATHICSE, Chair of Modelling and Scientific Computing, Ecole Polytechnique Fédérale de Lausanne, Station 8, CH-1015 Lausanne, Switzerland*

SUMMARY

This paper is concerned with ICDD (Interface Control Domain Decomposition) method, a strategy introduced for the solution of partial differential equations (PDEs) in computational domains partitioned into subdomains that overlap. After reformulating the original boundary value problem with the introduction of new additional control variables, the unknown traces of the solution at internal subdomain interfaces, the determination of the latter is made possible by the requirement that the (a-priori) independent solutions in each subdomain undergo a minimization of a suitable cost functional.
We illustrate the method on two kinds of boundary value problems, one homogeneous (an elliptic PDE), the other heterogeneous (a coupling between a second order advection-diffusion equation and a first order advection equation). We derive the associated optimality system, analyze its well posedness, and illustrate efficient algorithms based on the solution of the Schur-complement system restricted solely to the interface control variables. Finally, we validate numerically our method through a family of numerical tests and investigate the excellent convergence properties of our iterative solution algorithm.

KEY WORDS: Multifield Problems, Heterogeneous Problems, Domain Decomposition Methods, Advection-Diffusion, hp-Finite Elements, Spectral Elements

1. INTRODUCTION

ICDD (Interface Control Domain Decomposition) is a strategy for the solution of partial differential equations (PDEs) in computational domains partitioned into subdomains that overlap. It shares analogies and differences with similar strategies, most remarkably with that based on the Schwarz overlapping method (see [1, 2, 3]).

The distinguishing (and original) feature of ICDD method is that the original boundary value problem is reformulated with the help of new additional variables, the unknown traces of the solution at internal subdomain interfaces, that play the role of *control* variables. Their determination is made possible by the requirement that the (a-priori) independent solutions in each subdomain undergo a minimization of a suitable *cost functional*.

What distinguishes between different kinds of ICDD method is the role (and meaning) of the interface control variables - they can be either Dirichlet, or Neumann, or Robin traces of the subdomain unknowns - and the type of cost functional chosen - it can express different kinds of norm of the difference between the two solutions in overlapping areas or on internal interfaces.

*Correspondence to: Paola Gervasio, DICATAM, Università di Brescia, via Branze 38, I-25123 Brescia, Italy. E-mail: gervasio@ing.unibs.it

When the ICDD method is applied to classical (homogeneous) elliptic equations, as we do in the first part of this paper, it can be regarded as (yet) another domain decomposition (DD) method to solve elliptic problems. In fact, a specific version of it was early introduced in [4], then in [5] where the name of Virtual Control Methods was coined, and it was more recently revisited, generalized and optimized by the authors of this paper in [6, 7]. However, what makes it interesting in the version proposed in this paper, are its convergence properties of grid independence, robustness with respect to the possible variation of operator coefficients, and its built-in coarse global structure.

ICDD methods become especially attractive when applied to solve *heterogeneous* PDEs, that is coupled problems where different kinds of PDE are set up in different subdomains. A noticeable example is in multiphysics applications, in which case the different PDEs are designed to model different kinds of physics. Examples include fluid-structure interactions (modeled e.g. by Navier-Stokes equations coupled with the system of linear or nonlinear elasticity), the coupling between surface and subsurface flows (modeled e.g. by Stokes and Darcy equations [8, 9]), etc. In those cases, the minimization problem set on the interface control variables that is enforced by ICDD methods can in principle assure the correct matching between the two different physics without requiring the a-priori determination of the interface transmission conditions at the interface between them.

In this context, ICDD methods can be regarded not only as a new way to numerically solve a given boundary value problem, but also as a new (alternative) way to model multiphysics problems and, at the same time, provide a tool to find numerical solutions efficiently.

In this paper the heterogeneous problem considered is one arising from the coupling of an advection-diffusion equation with an advection equation, the latter being derived by the original equation by dropping the diffusion term in a subregion of the original computational domain.

The problem is simple but not too simple for testing the properties of the ICDD method.

In both cases (either homogeneous and heterogeneous) the given boundary value problem is reformulated as an *optimality system*, then reduced to an interface problem that depends solely on the interface control variables.

After replacing the interface problem by its discrete version (obtained using the hp-Galerkin approximation), we illustrate the solution algorithm and extensively analyze its rate of convergence as a function of the discretization parameters (the grid-space h and the polynomial degree p), the geometrical parameters (thickness of the overlapping area, number of subdomains in the partition), and the physical parameters (the piecewise constant values of the diffusion coefficient, the Péclet number of the advection-diffusion operator).

The ICDD method enjoys excellent convergence properties and represents a novel and fairly general paradigm to face both homogeneous and heterogeneous PDEs in domain decomposition environments.

The outline of the paper is as follows. In Section 2 we recall the setting and formulation of ICDD methods for homogeneous elliptic problems. In Section 3 we extend one special instance of ICDD methods (the one that shows the best convergence properties) to the case of heterogeneous coupling between Advection and Advection–Diffusion problems. In Section 4 we describe the reduction of the optimality systems associated to minimization problems to the interface control variables through the Schur-complement approach, moreover we reformulate ICDD methods algebraically. We conclude in Sections 5 and 6 by addressing a variety of test cases for both homogeneous and heterogeneous problems.

2. ICDD METHODS FOR ELLIPTIC PROBLEMS

Let $\Omega \subset \mathbb{R}^d$ $(d = 1, 2, 3)$ be an open bounded domain with boundary $\partial\Omega$, Γ_D and Γ_N two open subsets of $\partial\Omega$ such that $\partial\Omega = \overline{\Gamma_D \cup \Gamma_N}$ and $\Gamma_D \cap \Gamma_N = \emptyset$. Let L be the second order linear elliptic operator

$$Lu = \mathrm{div}(-\nu\nabla u + \mathbf{b}u) + \gamma u, \tag{1}$$

where $\nu \in L^\infty(\Omega)$ is such that $\exists \underline{\nu} > 0 : \ \nu(\mathbf{x}) \geq \underline{\nu} \, \forall \mathbf{x} \in \Omega$, while $\mathbf{b} \in [W^{1,\infty}(\Omega)]^d$ and $\gamma \in L^\infty(\Omega)$, with $\gamma(\mathbf{x}) \geq 0$ in Ω are such that the elliptic operator is coercive (see [10] for a detailed description of assumptions required).

Let us consider the boundary-value problem

Problem $\mathcal{P}$:

$$\begin{array}{ll} Lu = f & \text{in } \Omega \\ u = \phi_D & \text{on } \Gamma_D \\ \partial_{n_L} u = \phi_N & \text{on } \Gamma_N, \end{array} \tag{2}$$

where $f \in L^2(\Omega)$, $\phi_D \in H^{1/2}(\Gamma_D)$, $\phi_N \in H^{-1/2}(\Gamma_N)$ are assigned functions satisfying suitable compatibility conditions on $\Gamma_N \cap \Gamma_D$ (see [11]), and $\partial_{n_L} u$ denotes the conormal derivative of u:

$$\partial_{n_L} u = \nu \mathbf{n} \cdot \nabla u - \mathbf{b} \cdot \mathbf{n} u,$$

$\mathbf{n}$ being the unit normal vector external to $\partial\Omega$.

We split Ω into 2 overlapping subdomains Ω_1 and Ω_2 such that

$$\overline{\Omega} = \overline{\Omega_1 \cup \Omega_2},$$

then we set $\Omega_{12} = \Omega_1 \cap \Omega_2$, $\Gamma_i = \partial\Omega_{12} \setminus \partial\Omega_i$, $\Gamma_D^i = \Gamma_D \cap \partial\Omega_i$ and $\Gamma_N^i = \Gamma_N \cap \partial\Omega_i$ for $i = 1, \ 2$. See Fig. 1 for a simple example in $\mathbb{R}^2$.

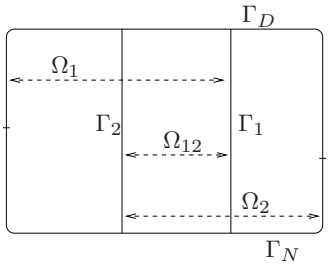

Figure 1. Partition of $\Omega \subset \mathbb{R}^2$ in two overlapping subdomains

We consider two multidomain formulations of *Problem* $\mathcal{P}_\Omega$:

Problem $\mathcal{P}_{\Omega_{12}}$:

$$\begin{array}{ll} Lu_1 = f & \text{in } \Omega_1 \\ Lu_2 = f & \text{in } \Omega_2 \\ u_1 = u_2 & \text{in } \Omega_{12}, \end{array} \tag{3}$$

Problem $\mathcal{P}_{\Gamma_1 \cup \Gamma_2}$:

$$\begin{array}{ll} Lu_1 = f & \text{in } \Omega_1 \\ Lu_2 = f & \text{in } \Omega_2 \\ \Psi(u_1) = \Psi(u_2) & \text{on } \Gamma_1 \cup \Gamma_2, \end{array} \tag{4}$$

both supplemented with boundary conditions

$$\begin{array}{ll} u_i = \phi_{D|\Gamma_D^i} & \text{on } \Gamma_D^i \ i = 1, 2, \\ \partial_{n_L} u_i = \phi_{N|\Gamma_N^i} & \text{on } \Gamma_N^i, \ i = 1, 2. \end{array} \tag{5}$$

We denote by $\Psi(u_i)$ either the trace of u_i on $\Gamma_1 \cup \Gamma_2$, or its conormal derivative $\partial_{n_L} u_i$ on $\Gamma_1 \cup \Gamma_2$, or else a linear combination between u_i and $\partial_{n_L} u_i$. Thus, depending on the choice of Ψ, condition $(4)_3$ may become, either

$$u_1 = u_2 \quad \text{on } \Gamma_1 \cup \Gamma_2, \tag{6}$$

(which stands at the base of Schwarz method) or

$$\partial_{n_L} u_1 = \partial_{n_L} u_2 \quad \text{on } \Gamma_1 \cup \Gamma_2, \tag{7}$$

or else

$$\beta u_1 + \partial_{n_L} u_1 = \beta u_2 + \partial_{n_L} u_2 \quad \text{on } \Gamma_1 \cup \Gamma_2, \tag{8}$$

where $\beta \geq 0$ is a suitable parameter. The equality (7) on Γ_1 should be understood as follows. The normal vector $\mathbf{n}$ on Γ_1 is directed outward of Ω_1 and the conormal derivative of u_2 is computed upon restricting u_2 to Ω_{12}. On the other hand, on Γ_2 the normal vector $\mathbf{n}$ is directed outward of Ω_2 and the conormal derivative of u_1 is taken upon restricting it to Ω_{12}.
Since (7) is a special case of (8) corresponding to $\beta = 0$, in the following we will consider only the more general condition (8).

The following result was proved in [10].

Proposition 2.1
Both problems (3) and (4) are equivalent to (2) in the sense that $u_i = u|_{\Omega_i}$, $i = 1, 2$. In particular, they are well-posed.

Even if multidomain formulations (3) and (4) share the same solution at the continuous level, they lead to different numerical methods, that behave in a different way with respect to the discretization parameters and the overlap thickness, as we will show in Section 5.

ICDD methods are designed to solve problems (3) and (4). They consist in introducing two control functions λ_1 and λ_2 which play the role of unknown Dirichlet (or Robin) data at the interfaces Γ_1 and Γ_2 of the decomposition and in minimizing the difference between the corresponding solutions u_1 and u_2 through a suitable cost functional defined on Ω_{12} (for problem (3)) or $\partial\Omega_{12} \setminus \partial\Omega = \Gamma_1 \cup \Gamma_2$ (for problem (4)).

For the sake of simplicity, we put $\Gamma_N = \emptyset$ (thus $\Gamma_D = \partial\Omega$) and $\phi_D = 0$. We define the following Hilbert spaces:

$$V_i = \{v_i \in H^1(\Omega_i) \,:\, v_i = 0 \text{ on } \Gamma_D^i\}, \quad V_i^D = \{v_i \in V_i \,:\, v_i = 0 \text{ on } \Gamma_i\}$$

endowed with the canonical norm of $H^1(\Omega_i)$, and $\mathbf{V} = V_1 \times V_2$, $\mathbf{V}^D = V_1^D \times V_2^D$, endowed with the corresponding graph norms.

For $i = 1, 2$, let us introduce the vector spaces of admissible *Dirichlet* controls

$$\Lambda_i^D = H_{00}^{1/2}(\Gamma_i) = \{\mu \in H^{1/2}(\Gamma_i) \,:\, \exists v \in H^1(\Omega_i),\ v = \mu \text{ on } \Gamma_i,\ v = 0 \text{ on } \Gamma_D^i\},$$

that are Hilbert spaces when endowed with the canonical norm in $H_{00}^{1/2}(\Gamma_i)$, and set $\mathbf{\Lambda}^D = \Lambda_1^D \times \Lambda_2^D$, endowed with the corresponding graph norm (see [12, 13]).

For $i = 1, 2$ we define the state problems:

$$\begin{aligned} &Lu_i^{\lambda_i, f} = f && \text{in } \Omega_i, \\ &u_i^{\lambda_i, f} = \lambda_i && \text{on } \Gamma_i, \\ &u_i^{\lambda_i, f} = 0 && \text{on } \partial\Omega_i \setminus \Gamma_i, \end{aligned} \tag{9}$$

moreover, we denote by $u_i^{\lambda_i} = u_i^{\lambda_i, 0}$ the solution of (9) with $f = 0$, and we set $\boldsymbol{\lambda} = [\lambda_1, \lambda_2]$ and $\mathbf{u}^{\boldsymbol{\lambda}} = [u_1^{\lambda_1}, u_2^{\lambda_2}]$. Because of problems linearity, $u_i^{\lambda_i, f} = u_i^{\lambda_i, 0} + u_i^{0, f}$, where $u_i^{0, f}$ is the solution of (9) with $\lambda_i = 0$.

Similarly, the Hilbert spaces of admissible *Robin* controls (with $\beta \geq 0$) are

$$\Lambda_i^R = (H_{00}^{1/2}(\Gamma_i))', \tag{10}$$

endowed with the canonical norm of $(H_{00}^{1/2}(\Gamma_i))'$ and set $\mathbf{\Lambda}^R = \Lambda_1^R \times \Lambda_2^R$, endowed with the corresponding graph norm.

In this case, (9) is replaced by

$$\begin{aligned} &Lu_i^{\lambda_i, f} = f && \text{in } \Omega_i, \\ &\beta u_i^{\lambda_i, f} + \partial_{n_L} u_i^{\lambda_i, f} = \lambda_i && \text{on } \Gamma_i \\ &u_i^{\lambda_i, f} = 0 && \text{on } \partial\Omega_i \setminus \Gamma_i, \end{aligned} \tag{11}$$

where now $\lambda_i \in \Lambda_i^R$ are the Robin controls and condition $(11)_2$ holds in Λ_i^R.

The interface controls are determined through the solution of a minimization problem as follows:

Case 1: Minimization in the norm $L^2(\Omega_{12})$:

$$\inf_{\lambda_1,\lambda_2} J_0(\lambda_1,\lambda_2), \quad \text{with } J_0(\lambda_1,\lambda_2) = \frac{1}{2}\|u_1^{\lambda_1,f} - u_2^{\lambda_2,f}\|^2_{L^2(\Omega_{12})}. \tag{12}$$

Case 2: Minimization in the norm $H^1(\Omega_{12})$:

$$\inf_{\lambda_1,\lambda_2} J_1(\lambda_1,\lambda_2), \quad \text{with } J_1(\lambda_1,\lambda_2) = \frac{1}{2}\|u_1^{\lambda_1,f} - u_2^{\lambda_2,f}\|^2_{H^1(\Omega_{12})}. \tag{13}$$

Case 3: Minimization in the norm $L^2(\Gamma_1 \cup \Gamma_2)$:

$$\inf_{\lambda_1,\lambda_2} J_{0,\Gamma}(\lambda_1,\lambda_2), \quad \text{with } J_{0,\Gamma}(\lambda_1,\lambda_2) = \frac{1}{2}\|u_1^{\lambda_1,f} - u_2^{\lambda_2,f}\|^2_{L^2(\Gamma_1\cup\Gamma_2)}. \tag{14}$$

Each functional defined in (12) – (14) can be rewritten in the general form

$$J_*(\lambda_1,\lambda_2) = \frac{1}{2}\|u_1^{\lambda_1,f} - u_2^{\lambda_2,f}\|^2_*, \tag{15}$$

where $\|\cdot\|_*$ is the canonical norm on the observation space V_*, which is either $L^2(\Omega_{12})$ or $H^1(\Omega_{12})$ or $L^2(\Gamma_1 \cup \Gamma_2)$, respectively in Case 1, 2 or 3.

The minimization problems (12), (13) and (14) with constraints (9) (or (11)) are in fact optimal control problems and they can be analyzed by using the classical theory of optimization (see, e.g., [14]). The controls are of boundary type (actually they are interface controls); the observation is distributed on the overlap in both (12) and (13), while it is of boundary type in (14).

Problems (12) and (13) with constraints (9) were proposed in the papers by Glowinski et al. [4] and Lions et al. [5], without however being analyzed. In [4] these methods were called *Least-Squares Conjugate-Gradient Methods*, while in [5] they were named *Virtual Control Methods*. The latter nomenclature has been used also by the authors of this paper in previous works (see [7, 6]).

Since J_* is convex, the classical way to prove that J_* admits a unique minimizer consists in:

1. proving that $\|u_1^{\lambda_1} - u_2^{\lambda_2}\|_* = |\!|\!|\boldsymbol{\lambda}|\!|\!|_*$ is a norm on the space $\boldsymbol{\Lambda}$ (either $\boldsymbol{\Lambda}^D$ or $\boldsymbol{\Lambda}^R$) of the controls;
2. considering the completion $\widehat{\boldsymbol{\Lambda}}$ of $\boldsymbol{\Lambda}$ with respect to the norm $|\!|\!|\cdot|\!|\!|_*$. As a matter of fact, it is not guaranteed that the space $\boldsymbol{\Lambda}$ is complete w.r.t. to the norm $|\!|\!|\cdot|\!|\!|_*$. Notice that the abstract space obtained by completion can be "very large", however this is not an issue when using finite dimensional approximations, as we will see in Section 4 (see (37) and (38)).;
3. writing the Euler-Lagrange (EL) equation

$$\langle\!\langle J_*'(\boldsymbol{\lambda}), \boldsymbol{\mu}\rangle\!\rangle = (u_1^{\lambda_1,f} - u_2^{\lambda_2,f}, u_1^{\mu_1} - u_2^{\mu_2})_* = 0 \quad \forall \boldsymbol{\mu} \in \widehat{\boldsymbol{\Lambda}}, \tag{16}$$

   where $\widehat{\boldsymbol{\Lambda}}$ stands for either $\widehat{\boldsymbol{\Lambda}}^D$ or $\widehat{\boldsymbol{\Lambda}}^R$, while $\langle\!\langle\cdot,\cdot\rangle\!\rangle$ denotes the duality between $\widehat{\boldsymbol{\Lambda}}$ and its dual space, and $\langle\!\langle \boldsymbol{\lambda}, \boldsymbol{\mu}\rangle\!\rangle = \langle\lambda_1,\mu_1\rangle + \langle\lambda_2,\mu_2\rangle$;
4. proving by the Lax-Milgram Lemma that the EL equation (16) admits a unique solution.

The following result holds.

Proposition 2.2
In all Cases 1–3, $\|u_1^{\lambda_1} - u_2^{\lambda_2}\|_* = |\!|\!|\boldsymbol{\lambda}|\!|\!|_*$ is a norm on the control space $\boldsymbol{\Lambda}$ (either $\boldsymbol{\Lambda}^D$ or $\boldsymbol{\Lambda}^R$). Moreover, each one of the minimization problems (12) – (14) admits a unique solution $\boldsymbol{\lambda} \in \widehat{\boldsymbol{\Lambda}}$, that is the solution of the EL equation (16).

Proof. When Dirichlet controls are considered the proof is given in [10, Sect. 4]. The proof for Robin controls can be repeated following the same guidelines. As a matter of fact, the regularity of the state solutions of (11) with $\boldsymbol{\lambda} \in \boldsymbol{\Lambda}^R$ is the same of the solution of (9) with $\boldsymbol{\lambda} \in \boldsymbol{\Lambda}^D$. The other arguments of the proof can be used in the same way. □

For $i = 1, 2$ we define the bilinear forms $a_i : V_i \times V_i \to \mathbb{R}$

$$a_i(u_i, v_i) = \int_{\Omega_i} (\nu \nabla u_i - \mathbf{b} u_i) \cdot \nabla v_i + \int_{\Omega_i} \gamma u_i v_i \tag{17}$$

and the linear functionals $F_i : V_i \to \mathbb{R}$

$$F_i(v_i) = \int_{\Omega_i} f v_i. \tag{18}$$

The computation of the minimizer $\boldsymbol{\lambda}$ can be achieved by solving the *Optimality System (OS)* associated to (16), that we report below.

In the case of Dirichlet controls the OS reads:

Cases 1-2: find $\mathbf{u} \in \mathbf{V}$, $\mathbf{p} \in \mathbf{V}^D$, $\boldsymbol{\lambda} \in \widehat{\boldsymbol{\Lambda}}^D$ such that for $i = 1, 2$ with $j = 3 - i$:

$$\begin{aligned} &a_i(u_i, v_i) = F_i(v_i), \quad u_i = \lambda_i \text{ on } \Gamma_i && \forall v_i \in V_i^D \\ &a_i(v_i, p_i) = (u_i - u_j, v_i)_* && \forall v_i \in V_i^D \\ &\langle\!\langle [\partial_{n_L} p_1, \partial_{n_L} p_2], \boldsymbol{\mu} \rangle\!\rangle = 0 && \forall \boldsymbol{\mu} = (\mu_1, \mu_2) \in \widehat{\boldsymbol{\Lambda}}^D; \end{aligned} \tag{19}$$

Case 3: find $\mathbf{u}, \mathbf{p} \in \mathbf{V}$, $\boldsymbol{\lambda} \in \widehat{\boldsymbol{\Lambda}}^D$ such that for $i = 1, 2$ with $j = 3 - i$:

$$\begin{aligned} &a_i(u_i, v_i) = F_i(v_i), \quad u_i = \lambda_i \text{ on } \Gamma_i && \forall v_i \in V_i^D \\ &a_i(p_i, v_i) = 0, \quad p_i = (u_i - u_j) \text{ on } \Gamma_i && \forall v_i \in V_i^D \\ &\sum_{i=1}^{2} \int_{\Gamma_i} ((u_i - u_j) + p_j) \mu_i d\Gamma = 0 && \forall \boldsymbol{\mu} = (\mu_1, \mu_2) \in \widehat{\boldsymbol{\Lambda}}^D. \end{aligned} \tag{20}$$

In the case of Robin controls the OS reads:

Cases 1-2: find $\mathbf{u} \in \mathbf{V}$, $\mathbf{p} \in \mathbf{V}$, $\boldsymbol{\lambda} \in \widehat{\boldsymbol{\Lambda}}^R$ such that for $i = 1, 2$ with $j = 3 - i$:

$$\begin{aligned} &a_i(u_i, v_i) + \int_{\Gamma_i} \beta u_i v_i = F_i(v_i) + \langle \lambda_i, v_i|_{\Gamma_i} \rangle && \forall v_i \in V_i \\ &a_i(v_i, p_i) + \int_{\Gamma_i} \beta v_i p_i = (u_i - u_j, v_i)_* && \forall v_i \in V_i \\ &\langle\!\langle \boldsymbol{\mu}, [p_1, p_2] \rangle\!\rangle = 0 && \forall \boldsymbol{\mu} \in \widehat{\boldsymbol{\Lambda}}^R; \end{aligned} \tag{21}$$

Case 3: find $\mathbf{u} \in \mathbf{V}$, $\mathbf{p} \in \mathbf{V}$, $\boldsymbol{\lambda} \in \widehat{\boldsymbol{\Lambda}}^R$ such that for $i = 1, 2$ with $j = 3 - i$:

$$\begin{aligned} &a_i(u_i, v_i) + \int_{\Gamma_i} \beta u_i v_i = F_i(v_i) + \langle \lambda_i, v_i|_{\Gamma_i} \rangle && \forall v_i \in V_i \\ &a_i(p_i, v_i) + \int_{\Gamma_i} \beta p_i v_i = \int_{\Gamma_i} (u_i - u_j) v_i && \forall v_i \in V_i \\ &\langle\!\langle \boldsymbol{\mu}, [u_1 - u_2 + p_2, u_2 - u_1 + p_1] \rangle\!\rangle = 0 && \forall \boldsymbol{\mu} \in \widehat{\boldsymbol{\Lambda}}^R. \end{aligned} \tag{22}$$

Both OS (19) and (21) are obtained starting by the Euler-Lagrange equation (16) and integrating by parts. Therefore the dual states p_i are the solutions of elliptic problems which are dual of the primal state problems (9) (or (11)).

On the contrary, both OS (20) and (22) are not obtained by integration by parts. They have been defined in order to guarantee existence and uniqueness of minimizer (e.g., see theorem 4.3 of [10] for the Dirichlet case) and the functions p_i are the solutions of state problems of the same nature (and not dual) of either (9) or (11).

Remark 2.1
When applying ICDD methods to decompositions of Ω using $M > 2$ subdomains, we distinguish between strip-wise decompositions, when each overlapped region is shared only by two subdomains, and cross-wise decompositions, in which more than two subdomains can share a non-empty region. In the former case the subdomains Ω_k for $k = 1, \ldots, M$ can be numbered sequentially, so that all the odd (even, resp.) subdomains can be grouped in a unique disconnected subdomain $\widetilde{\Omega}_1$ ($\widetilde{\Omega}_2$, resp.) and the analysis presented above still holds provided Ω_i is replaced by $\widetilde{\Omega}_i$ (for $i = 1, 2$). Otherwise in the latter case, we define $\Omega_{ij} = \Omega_i \cap \Omega_j$ for $i \neq j$ and replace the cost functionals (15) by

$$J_*(\boldsymbol{\lambda}) = \frac{1}{2} \sum_{\substack{i,j=1 \\ i>j \\ \Omega_{ij}\neq\emptyset}}^{M} \|u_i^{\lambda_i,f} - u_j^{\lambda_j,f}\|_{*,ij}^2 \tag{23}$$

where $*, ij$ stands for $L^2(\Omega_{ij})$, $H^1(\Omega_{ij})$ or $L^2(\partial\Omega_{ij})$. The formulation of OS (19)–(20) and (21)–(22) follows by replacing Ω_{12} with Ω_{ij} for any $i, j = 1, \ldots, M$ and counting every overlapping area once.

We refer to [15] for the analysis of the convergence rate of ICDD methods for elliptic selfadjoint problems.

In the next Section we introduce ICDD methods for heterogeneous PDEs, namely an Advection – Advection/Diffusion coupled problem. We will come back to the homogeneous case addressed until now (i.e. one with the same differential operator in both subdomains) in Section 4, where we will formulate the discretization of the OS (19) – (20), and in Section 5 where we report numerical results validating the robustness of ICDD methods with respect to the variations of the coefficients of the problem.

3. ICDD FOR THE COUPLING OF ADVECTION WITH ADVECTION/DIFFUSION PROBLEMS

Let us consider the coupling of Advection and Advection/Diffusion equations (in brief A–AD), that is of interest when considering a global advection-diffusion problem with dominating advective field, whose solution features internal and/or boundary layers (see Fig. 2). In such a case the presence of the viscous term might not be essential far from the layer; by dropping it yields a reduced order differential operator in the latter region.

We decompose the computational domain Ω as described in Section 2, therefore we look for two functions u_1 and u_2 (defined in $\overline{\Omega}_1$ and $\overline{\Omega}_2$, respectively) such that u_1 satisfies the advection equation

$$\widetilde{L}u_1 = \mathrm{div}(\mathbf{b}u_1) + \gamma u_1 = f, \qquad \text{in } \Omega_1, \tag{24}$$

while u_2 satisfies the advection-diffusion equation

$$Lu_2 = f, \qquad \text{in } \Omega_2, \tag{25}$$

where L is defined in (1).

The boundary conditions for the subproblems are inherited by the original one by taking care of the advective problem in Ω_1. As a matter of fact the first-order problem is well posed only when the Dirichlet condition is assigned on the *inflow* boundary $(\partial\Omega_1)^{in}$, where for any non-empty subset $\Gamma \subseteq \partial\Omega_1$, we set

$$\text{the } \textit{inflow} \text{ part of } \Gamma: \quad \Gamma^{in} = \{\mathbf{x} \in \Gamma : \mathbf{b}(\mathbf{x}) \cdot \mathbf{n}(\mathbf{x}) < 0\},$$

$$\text{the } \textit{outflow} \text{ part of } \Gamma: \quad \Gamma^{out} = \{\mathbf{x} \in \Gamma : \mathbf{b}(\mathbf{x}) \cdot \mathbf{n}(\mathbf{x}) > 0\}$$

and

$$\Gamma^0 = \Gamma \setminus (\overline{\Gamma^{in}} \cup \overline{\Gamma^{out}}).$$

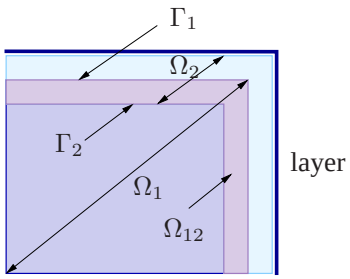

Figure 2. Graphic representation of a 2D A-AD heterogeneous coupling

Therefore we assume that $(\partial\Omega_1 \setminus \Gamma_1)^{in} \subset \Gamma_D$, we set $\Gamma_2^{nz} = \Gamma_2 \setminus \Gamma_2^0$ and define the heterogeneous
Problem $\mathcal{P}^H_{\Gamma_1\cup\Gamma_2}$:

$$\begin{array}{ll} \widetilde{L}u_1 = f & \text{in } \Omega_1 \\ Lu_2 = f & \text{in } \Omega_2 \\ u_1 = u_2 & \text{on } \Gamma_1^{in} \cup \Gamma_2^{nz} \\ u_1 = \phi_D & \text{on } (\partial\Omega_1 \setminus \Gamma_1)^{in} \\ \nu\dfrac{\partial u_2}{\partial n_2} = 0 & \text{on } \Gamma_2^0 \\ u_2 = \phi_D & \text{on } \Gamma_D^2 \\ \partial_{n_L} u_2 = \phi_N & \text{on } \Gamma_N^2. \end{array} \tag{26}$$

Notice that the interface condition for Ω_1 is assigned only on the inflow part of the interface Γ_1, while that for Ω_2 is given on the subset of Γ_2 where $\mathbf{b}\cdot\mathbf{n} \neq 0$.

The analogous of problem (3) is not considered in this context, since in general there is no guarantee that $u_1 = u_2$ in Ω_{12} for heterogeneous problems (see, e.g., [7, 16]).

A preliminary study of the A–AD coupling with overlapping subdomains has been carried out in [7, 16, 6, 10]. Following the formalism introduced in [10], we are going now to define the ICDD method with interface observation and to analyze it.

First, we introduce some useful spaces. Given an open domain $D \subset \mathbb{R}^d$ with Lipschitz boundary ∂D and given $S \subseteq \partial D$, we define

$$L^2_{\mathbf{b}}(S) = \{v : S \to \mathbb{R} : \ v\sqrt{|\mathbf{b}\cdot\mathbf{n}_S|} \in L^2(S)\}, \tag{27}$$

where $\mathbf{n}_S$ denotes the outward normal versor to S, and

$$X_{\mathbf{b}}(D) = \{v \in L^2(D),\ \mathrm{div}(\mathbf{b}v) \in L^2(D) : \ v \in L^2_{\mathbf{b}}(\partial D)\}. \tag{28}$$

They are both Hilbert spaces (see [17]) with respect to their natural norms:

$$\|u\|_{L^2_{\mathbf{b}}(S)} = \left(\int_S |\mathbf{b}\cdot\mathbf{n}|u^2 dS\right)^{1/2}, \ \|u\|_{X_{\mathbf{b}}(D)} = \left(\|u\|^2_{L^2(D)} + \|\mathrm{div}(\mathbf{b}u)\|^2_{L^2(D)} + \|u\|^2_{L^2_{\mathbf{b}}(\partial D)}\right)^{1/2}.$$

Finally, we define the spaces of the controls:

$$\Lambda_1 = L^2_{\mathbf{b}}(\Gamma_1^{in}), \qquad \Lambda_2 = H^{1/2}_{00}(\Gamma_2^{nz}).$$

The ICDD formulation for the heterogeneous coupling (26) reads as follows (see Figure 2): look for the interface controls $\lambda_1 \in \Lambda_1$ and $\lambda_2 \in \Lambda_2$ solutions of

$$\inf_{\lambda_1,\lambda_2} J_{\mathbf{b}}(\lambda_1,\lambda_2) \quad \text{with} J_{\mathbf{b}}(\lambda_1,\lambda_2) = \frac{1}{2}\int_{\Gamma_1^{in}\cup\Gamma_2^{nz}} |\mathbf{b}\cdot\mathbf{n}|(u_1^{\lambda_1,f} - u_2^{\lambda_2,f})^2, \tag{29}$$

where $u_1^{\lambda_1,f}$ and $u_2^{\lambda_2,f}$ are the solutions of

$$\begin{array}{ll} \widetilde{L}u_1^{\lambda_1,f} = f & \text{in } \Omega_1 \\ u_1^{\lambda_1,f} = 0 & \text{on } (\partial\Omega_1 \setminus \Gamma_1)^{in} \\ u_1^{\lambda_1,f} = \lambda_1 & \text{a.e. on } \Gamma_1^{in}, \end{array} \qquad \begin{array}{ll} Lu_2^{\lambda_2,f} = f & \text{in } \Omega_2 \\ u_2^{\lambda_2,f} = 0 & \text{on } \partial\Omega_2 \setminus \Gamma_2 \\ u_2^{\lambda_2,f} = \lambda_2 & \text{on } \Gamma_2^{nz} \\ \partial_{n_L} u_2^{\lambda_2,f} = 0 & \text{on } \Gamma_2^0. \end{array} \tag{30}$$

We require that $\exists \beta_0 > 0$ such that $\frac{1}{2}\nabla \cdot \mathbf{b} + \gamma \geq \beta_0$ in Ω_1, to ensure the first-order problem in (30) has unique solution.

Thanks to the regularity of the data, it holds $u_2^{\lambda_2,f} \in H^1(\Omega_2)$, while $u_1^{\lambda_1,f} \in X_{\mathbf{b}}(\Omega_1)$, moreover if S coincides with either Γ_1^{in} or Γ_2^{nz}, it holds $H^{1/2}(S) \subset L^2_{\mathbf{b}}(S)$, then the integrals in (29) are bounded and the definition of $J_{\mathbf{b}}$ makes sense.

As done for the homogeneous elliptic case, since both $\widetilde{L}$ and L are linear, we can write $u_i^{\lambda_i,f} = u_i^{\lambda_i} + u_i^{0,f}$ (for $i = 1, 2$), where $u_1^{\lambda_1}$ and $u_2^{\lambda_2}$ are the solution of (30) with $f = 0$, then we set $\boldsymbol{\lambda} = (\lambda_1, \lambda_2)$ and $\mathbf{u}^{\boldsymbol{\lambda}} = (u_1^{\lambda_1}, u_2^{\lambda_2})$.

We define

$$\widetilde{V}_1 = X_{\mathbf{b}}(\Omega_1), \quad \widetilde{V}_1^D = \{v \in \widetilde{V}_1 : \ v|_{(\partial\Omega_1 \setminus \Gamma_1)^{in}} = 0\},$$

we take V_2 and V_2^D as in Section 2 and we set $\mathbf{V}_H = \widetilde{V}_1 \times V_2$, $\mathbf{V}_H^D = \widetilde{V}_1^D \times V_2^D$ and $\boldsymbol{\Lambda}_H = \Lambda_1 \times \Lambda_2$. Finally we define the bilinear form $\widetilde{a} : \widetilde{V}_1 \times \widetilde{V}_1 \to \mathbb{R}$:

$$\widetilde{a}(u_1, v_1) = -\int_{\Omega_1} u_1 \mathbf{b} \cdot \nabla v_1 + \int_{\Omega_1} \gamma u_1 v_1 + \int_{\partial\Omega_1^{out}} \mathbf{b} \cdot \mathbf{n} u_1 v_1.$$

The Euler-Lagrange equation $\langle J'_{\mathbf{b}}(\boldsymbol{\lambda}), \boldsymbol{\mu}\rangle = 0$ associated to the minimization problem (29)–(30) reads:

$$\int_{\Gamma_1^{in} \cup \Gamma_2^{nz}} |\mathbf{b} \cdot \mathbf{n}|(u_1^{\lambda_1,f} - u_2^{\lambda_2,f})(u_1^{\mu_1} - u_2^{\mu_2}) = 0 \ \ \forall \boldsymbol{\mu} \in \boldsymbol{\Lambda}_H \tag{31}$$

while the optimality system reads: find $\mathbf{u}, \mathbf{p} \in \mathbf{V}_H$, $\boldsymbol{\lambda} \in \boldsymbol{\Lambda}_H$ such that

$$\begin{array}{llll} a_1(u_1, v_1) = F_1(v_1) & \forall v_1 \in V_1^D, & u_1 = \lambda_1 \ \text{ a.e. on } \Gamma_1^{in}, & \\ a_2(u_2, v_2) = F_2(v_2) & \forall v_2 \in V_2^D, & u_2 = \lambda_2 \ \text{ on } \Gamma_2^{nz}, & \nu \dfrac{\partial u_2}{\partial n_2} = 0 \ \text{ on } \Gamma_2^0 \\ a_1(p_1, v_1) = 0 & \forall v_1 \in V_1^D, & p_1 = u_1 - u_2 \ \text{ a.e. on } \Gamma_1^{in} & \\ a_2(p_2, v_2) = 0 & \forall v_2 \in V_2^D, & p_2 = u_2 - u_1 \ \text{ on } \Gamma_2^{nz}, & \nu \dfrac{\partial p_2}{\partial n_2} = 0 \ \text{ on } \Gamma_2^0 \end{array}$$
$$\int_{\Gamma_1^{in}} |\mathbf{b} \cdot \mathbf{n}|((u_1 - u_2) + p_2)\mu_1 d\Gamma + \int_{\Gamma_2^{nz}} |\mathbf{b} \cdot \mathbf{n}|((u_2 - u_1) + p_1)\mu_2 d\Gamma = 0 \quad \forall \boldsymbol{\mu} \in \boldsymbol{\Lambda}_H. \tag{32}$$

Remark 3.1

When the computational domain is partitioned in two non-overlapping subdomains Ω_1, Ω_2 with sharp interface (i.e. such that $\overline{\Omega}_1 \cup \overline{\Omega}_2 = \overline{\Omega}$, $\Omega_1 \cap \Omega_2 = \emptyset$ and $\Gamma = \partial\Omega_1 \cap \partial\Omega_2$), the heterogeneous A–AD coupling has been analyzed in [17, 18, 6, 19]. In [17, 19] the authors provided a suitable set of interface conditions on the sharp interface Γ of the decomposition, i.e.

$$\begin{array}{ll} u_1 = u_2 & \text{on } \Gamma^{in} \\ \mathbf{b} \cdot \mathbf{n} u_1 + \nu \mathbf{n} \cdot \nabla u_2 - \mathbf{b} \cdot \mathbf{n} u_2 = 0 & \text{on } \Gamma \end{array} \tag{33}$$

where $\mathbf{n}$ is the unit normal vector to Γ oriented from Ω_1 to Ω_2.

These conditions express the continuity of the velocity field across the *inflow* part of the unique interface Γ and the continuity of the fluxes across the whole interface Γ. In such case a suitable version of the classical Dirichlet-Neumann method ([20, 17]) is applied to solve the heterogeneous problem.

Other domain decomposition approaches based on virtual controls or extended variational formulation on non-overlapping subdomains have been addressed in [6, 18, 21] to face similar heterogeneous coupled problems.

4. DISCRETIZATION

In this Section we briefly address the discretization of the differential equations and the solution of the associated optimality systems (19) – (20) and (21) – (22) in discrete form.

Both primal and dual differential problems in each subdomain are discretized by hp Finite Element Methods (hp-FEM).

4.1. hp-FEM discretization

For $i = 1, 2$, let $\mathcal{T}_i$ be a partition of the computational domain $\Omega_i \subset \mathbb{R}^d$ in either simplexes or quadrilaterals/hexahedra (quadrilaterals when $d = 2$ and hexahedra when $d = 3$). We denote by $\hat{T}$ the reference element, that can be either the reference simplex with vertexes $\mathbf{0}$ and the points on the axis whose distance from the origin is 1, or the $d-$dimensional cube $(-1, 1)^d$.

We name *simplicial* the partitions composed by simplexes and *quad* those partitions formed by quadrilaterals/hexahedra. The first ones are typical of classical FEM, the others of Spectral Elements Methods (SEM) with tensorial structure (see [22, 23]).

We suppose that each element $T \in \mathcal{T}_i$ is obtained by a C^1 diffeomorphism $\mathbf{F}_T$ of the reference element $\hat{T}$ and we suppose that two adjacent elements of $\mathcal{T}_i$ share either a common vertex or a complete edge or a complete face (when $d = 3$). For each $T \in \mathcal{T}_i$ we denote by $h_T = \text{diam}(T) = \max_{\mathbf{x},\mathbf{y}\in T} |\mathbf{x} - \mathbf{y}|$ the diameter of element T and we define $h_i = \max_{T\in\mathcal{T}_i} h_T$. Then, when simplicial partitions are considered, we require that the grid is regular in each Ω_i (see, e.g., [13]).

Given an integer $p \geq 1$, let us denote by $\mathbb{P}_p$ the space of polynomials whose global degree is less than or equal to p in the variables $x_1, \ldots, x_d$ and by $\mathbb{Q}_p$ the space of polynomials that are of degree less than or equal to p with respect to each variable $x_1, \ldots, x_d$. The space $\mathbb{P}_p$ is associated to simplicial partitions, while $\mathbb{Q}_p$ to quad ones.

The finite dimensional space on $\overline{\Omega}_i$ is defined by

$$X_{i,\delta_i} = \{v \in C^0(\overline{\Omega}_i) \,:\, v_{|T} \circ \mathbf{F}_T \in \mathbb{P}_p,\ \forall T \in \mathcal{T}_i\} \tag{34}$$

in the simplicial case and by

$$X_{i,\delta_i} = \{v \in C^0(\overline{\Omega}_i) \,:\, v_{|T} \circ \mathbf{F}_T \in \mathbb{Q}_p,\ \forall T \in \mathcal{T}_i\}, \tag{35}$$

for quads, and we set $N_{\Omega_i} = \dim(X_{i,\delta_i})$.

The parameter δ_i is an abridged notation for "discrete", that accounts for the local geometric size h_i and the local polynomial degree p.

Finally, let M_i be the set of the nodes $\mathbf{x}_j$ of the mesh in Ω_i and $\mathsf{M}_{\Gamma_i} \subset \mathsf{M}_i$ the set of nodes $\mathbf{x}_j \in \mathsf{M}_i \cap \Gamma_i$, we denote by N_{Ω_i} and N_{Γ_i} their cardinality, respectively, and by $\mathcal{I}_i = \{1, \ldots, N_{\Omega_i}\}$ and $\mathcal{G}_i = \{j \in \mathcal{I}_i \,:\, \mathbf{x}_j \in \mathsf{M}_{\Gamma_i}\}$ the corresponding sets of indices.

For quads the mesh M_i is built by mapping the nodes of the Legendre-Gauss-Lobatto (LGL) quadrature formulas from $\hat{T}$ to the generic T through the mappings $\mathbf{F}_T$, in order to ensure exponential decay for both interpolation and quadrature errors ([22]).

The finite dimensional spaces in which we look for the hp-FEM solution are defined as follows:

$$\begin{aligned}
&V_{i,\delta_i} = V_i \cap X_{i,\delta_i}, \quad V^D_{i,\delta_i} = V^D_i \cap X_{i,\delta_i},\\
&\Lambda^D_{i,\delta_i} = \{\lambda_{i,\delta_i} \in C^0(\Gamma_i) : \exists\, v_{i,\delta_i} \in V_{i,\delta_i} \text{ with } \lambda_{i,\delta_i} = v_{i,\delta_i|\Gamma_i}\},\\
&\Lambda^R_{i,\delta_i} = \{\lambda_{i,\delta_i} \in L^2(\Gamma_i) : \exists\, v_{i,\delta_i} \in V_{i,\delta_i} \text{ with } \lambda_{i,\delta_i} = \partial_{n_L} v_{i,\delta_i} + \beta v_{i,\delta_i} \text{ on } \Gamma_i\}.
\end{aligned} \tag{36}$$

Then Λ^D_{i,δ_i} is a subspace of Λ^D_i and Λ^R_{i,δ_i} a subspace of Λ^R_i, and therefore

$$\boldsymbol{\Lambda}^D_\delta = \Lambda^D_{1,\delta_1} \times \Lambda^D_{2,\delta_2} \subset \boldsymbol{\Lambda}^D \subseteq \widehat{\boldsymbol{\Lambda}}^D. \tag{37}$$

Similarly,

$$\boldsymbol{\Lambda}^R_\delta = \Lambda^R_{1,\delta_1} \times \Lambda^R_{2,\delta_2} \subset \boldsymbol{\Lambda}^R \subseteq \widehat{\boldsymbol{\Lambda}}^R. \tag{38}$$

In V_{i,δ_i} we consider the basis of the characteristic Lagrange polynomials

$$\mathcal{B}_{\Omega_i} = \{\varphi_{i,j},\ \text{with } j \in \mathcal{I}_i\}$$

associated to the mesh M_i.

Moreover, we denote by $\mathcal{B}_{\Gamma_i}$ the finite dimensional basis in Λ^D_{i,δ_i} such that each basis function $\mu_{i,j}$ is the restriction to Γ_i of a suitable basis function of V_{i,δ_i} that is not identically null on Γ_i, i.e.

$$\mathcal{B}_{\Gamma_i} = \{\mu_{i,j} = \varphi_{i,j}|_{\Gamma_i},\ \text{with } j \in \mathcal{G}_i\}.$$

It follows that the *discrete Dirichlet controls* will be identified by the real (nodal) values

$$(\lambda_{i,\delta_i})_j = \lambda_{i,\delta_i}(\mathbf{x}_j), \quad \text{with } j \in \mathcal{G}_i. \tag{39}$$

The characterization of the discrete Robin controls requires more care.

Let $T_k \subset \Omega_i$ be the generic element in Ω_i, we introduce the set

$$\mathcal{E}_i = \{k :\ \text{meas}(\partial T_k \cap \Gamma_i) > 0\}$$

and, for any $k \in \mathcal{E}_i$, the edges $e_{ik} = \partial T_k \cap \Gamma_i$. Thanks to definition of $X_{i,\delta}$, for any $v_{i,\delta_i} \in X_{i,\delta_i}$ it holds $v_{i,\delta_i}|_{\overline{T}_k} \in C^1(\overline{T}_k)$ and then $\partial_{n_L} v_{i,\delta_i}$ makes sense on e_{ik}.

In view of definition (36)$_3$, for any $\mu_{i,j} \in \mathcal{B}_{\Gamma_i}$ and $\lambda_{i,\delta_i} \in \Lambda^R_{i,\delta_i}$,

$$\langle \lambda_{i,\delta_i}, \mu_{i,j} \rangle = \sum_{k \in \mathcal{E}_i} \int_{e_{ik}} \lambda_{i,\delta_i}\ \mu_{i,j}, \tag{40}$$

then the nodal values of the *discrete Robin controls* are given by

$$(\lambda_{i,\delta_i})_j = \sum_{k \in \mathcal{E}_i} \int_{e_{ik}} \lambda_{i,\delta_i}\ \mu_{i,j}, \quad \text{with } j \in \mathcal{G}_i. \tag{41}$$

By a similar argument, starting from

$$\langle\!\langle [\partial_{n_L} p_1, \partial_{n_L} p_2], \boldsymbol{\mu} \rangle\!\rangle = \langle \partial_{n_L} p_1, \mu_1 \rangle + \langle \partial_{n_L} p_2, \mu_2 \rangle$$

for any $\boldsymbol{\mu} = [\mu_1, \mu_2] \in \widehat{\boldsymbol{\Lambda}}^D$, we can compute the left hand side of (19)$_3$ by using the following formula and (40) as follows. For any $j \in \mathcal{G}_i$

$$\langle \partial_{n_L} p_i, \mu_{i,j} \rangle = \sum_{\ell \in \mathcal{I}_i} p_{i,\delta_i}(\mathbf{x}_\ell) \langle \partial_{n_L} \varphi_{i,\ell}, \mu_{i,j} \rangle = \sum_{\ell \in \mathcal{I}_i} p_{i,\delta_i}(\mathbf{x}_\ell) \underbrace{\sum_{k \in \mathcal{E}_i} \int_{e_{ik}} \partial_{n_L} \varphi_{i,\ell}\ \mu_{i,j}}_{(D_i)_{j\ell}}. \tag{42}$$

The matrices associated to the bilinear forms a_i and the discrete inner products read:

$$(A_i)_{lj} = a_i(\varphi_{i,j}, \varphi_{i,l}), \quad (M_i)_{lj} = (\varphi_{i,j}, \varphi_{i,l})_{L^2(\Omega_i)}, \quad \text{for } l, j = 1, \ldots, N_{\Omega_i}.$$

Because of the difficulty to compute integrals exactly for large p, typically when quad partitions are used, Legendre-Gauss-Lobatto quadrature formulas are used to approximate both the bilinear forms a_i and the L^2-inner products in Ω_i (as well as on the interfaces). This leads to the so called *Galerkin approach with Numerical Integration* (G-NI) [22, 24] and to the Spectral Element Method with Numerical Integration (SEM-NI).

4.2. *Discretization and solution of the OS*

The OS has six unknown functions:
- the primal state variables $u_1,\ u_2$;
- the dual state variables $p_1,\ p_2$;
- the control variables $\lambda_1,\ \lambda_2$.

All the differential and integral equations of the OS are approximated by hp-FEM and u_{i,δ_i}, p_{i,δ_i}, λ_{i,δ_i} are the corresponding discrete solutions. Let $\mathsf{M}_i^0 \subset \mathsf{M}_i$ be the subset of the non-Dirichlet nodes of $\overline{\Omega}_i$ and $N_{\Omega_i}^0$ its cardinality. (We have eliminated Dirichlet nodes on both the external boundary and the interface.)

Let us denote by:

- $\mathbf{u}_i, \mathbf{p}_i \in \mathbb{R}^{N_{\Omega_i}^0}$, for $i = 1, 2$, the arrays whose entries are the values of the discrete primal states u_{i,δ_i} and of the discrete dual states p_{i,δ_i}, respectively, at the nodes in M_i^0;
- $\boldsymbol{\lambda}_i \in \mathbb{R}^{N_{\Gamma_i}}$, for $i = 1, 2$ the arrays of the values of the discrete control λ_{i,δ_i} at the nodes of $\mathsf{M}_i \cap \Gamma_i$, as defined in either (39) or (41).

For simplicity we consider the case of homogeneous Dirichlet conditions on the external boundary $\partial\Omega$, so that the external boundary degrees of freedom are dropped.

We start by analyzing the case with Dirichlet controls.

4.3. *Distributed observation. Dirichlet controls*

For $i = 1, 2$ we define the following matrices:

- A_{ii} is the submatrix of A_i obtained by selecting both rows and columns associated to the nodes of M_i^0;
- B_i is the submatrix of A_i obtained by selecting the rows associated to the nodes of M_i^0 and the columns associated to interface nodes of $\mathsf{M}_i \cap \Gamma_i$;
- C_i^0 and $C_i^{\Gamma_i}$ are submatrices of a matrix C_i which depends on whether we are minimizing either the cost functional (12) or (13). More precisely, for $l, j = 1, \ldots, N_{\Omega_i}^0$

$$(C_i)_{lj} = \begin{cases} (\varphi_{i,j}, \varphi_{i,l})_{L^2(\Omega_{12})} & \text{in Case 1} \\ (\varphi_{i,j}, \varphi_{i,l})_{H^1(\Omega_{12})} & \text{in Case 2.} \end{cases}$$

  Those columns of C_i associated to nodes on Γ_i are stored in $C_i^{\Gamma_i}$, the others in C_i^0;
- D_i are the matrices associated to the discretization of the last equation of the OS, as defined in (42).

Therefore, we set

$$A = \begin{bmatrix} A_{11} & 0 \\ 0 & A_{22} \end{bmatrix},\ B = \begin{bmatrix} B_1 & 0 \\ 0 & B_2 \end{bmatrix},\ C_0 = \begin{bmatrix} C_1^0 & -C_2^0 \\ -C_1^0 & C_2^0 \end{bmatrix},\ C_\Gamma = \begin{bmatrix} C_1^{\Gamma_1} & -C_2^{\Gamma_2} \\ -C_1^{\Gamma_1} & C_2^{\Gamma_2} \end{bmatrix}, \tag{43}$$

$$D = \begin{bmatrix} D_1 & 0 \\ 0 & D_2 \end{bmatrix},\ \mathbf{u} = \begin{bmatrix} \mathbf{u}_1 \\ \mathbf{u}_2 \end{bmatrix},\ \mathbf{p} = \begin{bmatrix} \mathbf{p}_1 \\ \mathbf{p}_2 \end{bmatrix},\ \boldsymbol{\lambda} = \begin{bmatrix} \boldsymbol{\lambda}_1 \\ \boldsymbol{\lambda}_2 \end{bmatrix},\ \mathbf{f} = \begin{bmatrix} \mathbf{f}_1 \\ \mathbf{f}_2 \end{bmatrix},$$

so that the matrix form of the OS (19) reads

$$\underbrace{\begin{bmatrix} A & 0 & B \\ C_0 & A^T & C_\Gamma \\ 0 & D & 0 \end{bmatrix}}_{G} \underbrace{\begin{bmatrix} \mathbf{u} \\ \mathbf{p} \\ \boldsymbol{\lambda} \end{bmatrix}}_{\mathbf{x}} = \underbrace{\begin{bmatrix} \mathbf{f} \\ \mathbf{0} \\ \mathbf{0} \end{bmatrix}}_{\mathbf{b}}. \tag{44}$$

By introducing the Schur-complement matrix S of G with respect to the control variable $\boldsymbol{\lambda}$

$$S_D = -\begin{bmatrix} 0 & D \end{bmatrix} \begin{bmatrix} A & 0 \\ C_0 & A^T \end{bmatrix}^{-1} \begin{bmatrix} B \\ C_\Gamma \end{bmatrix} = D(A^T)^{-1}(C_0 A^{-1} B - C_\Gamma) \tag{45}$$

and the vector

$$\boldsymbol{\psi}_D = D(A^T)^{-1} C_0 A^{-1} \mathbf{f}$$

the Schur-complement system associated to OS (44) reads

$$S_D \boldsymbol{\lambda} = \boldsymbol{\psi}_D \tag{46}$$

and it can be regarded as the discrete counterpart of the Euler equation (16) (see [10, Sect. 4.1]).

Since C_0 is singular and the (3,3)-block of G is null, any other block elimination of either $(\mathbf{p}, \boldsymbol{\lambda})$ or $(\mathbf{u}, \boldsymbol{\lambda})$ from system (44) would lead to ill-posed Schur-complement matrices.

The solution of the Schur-complement system (46) can be efficiently computed by Krylov methods as, e.g., Bi-CGStab ([25]), preconditioned whenever this is convenient.

At the kth Bi-CGStab iteration, if $\boldsymbol{\lambda}^{(k)}$ is a known array, the computation of the matrix-vector product $\boldsymbol{\chi}^{(k)} = S_D \boldsymbol{\lambda}^{(k)}$ is performed by the following algorithm which, in fact, reflects the three steps of the OS.

Algorithm 4.1 (Schur-complement evaluation)
Distributed observation - Dirichlet controls. Given $\boldsymbol{\lambda}^{(k)}$, compute $\boldsymbol{\chi}^{(k)} = S_D \boldsymbol{\lambda}^{(k)}$

1. solve $A\mathbf{u}^{(k)} = -B\boldsymbol{\lambda}^{(k)}$, i.e. use $\boldsymbol{\lambda}^{(k)}$ as Dirichlet data on the interfaces Γ_i and null functions F_i to solve primal states problems and find $\mathbf{u}^{(k)}$;
2. solve $A^T\mathbf{p}^{(k)} = C_0\mathbf{u}^{(k)}$, i.e., use $\mathbf{u}^{(k)}$ to assemble the right hand side for the dual state problems and find $\mathbf{p}^{(k)}$;
3. compute $\boldsymbol{\chi}^{(k)} = D\mathbf{p}^{(k)}$, i.e. compute the normal derivatives of $p_{i,\delta}^{(k)}$ at the interfaces Γ_i.

The right hand side $\boldsymbol{\psi}_D$ is computed off-line (once and for all) by a similar algorithm:

Algorithm 4.2 ($\boldsymbol{\psi}_D$ evaluation)
Distributed observation - Dirichlet controls. Given $\mathbf{f}$, compute $\boldsymbol{\psi}_D$

1. solve $A\mathbf{u}^f = \mathbf{f}$, i.e. use null Dirichlet data on the interfaces Γ_i and F_i as in (18) to solve primal states problems and find $\mathbf{u}^f$;
2. solve $A^T\mathbf{p}^f = C_0\mathbf{u}^f$;
3. compute $\boldsymbol{\psi}_D = D\mathbf{p}^f$.

The most expensive part of Algorithm 4.1 is the solution of both primal and dual problems, thus one matrix-vector product $S_D\boldsymbol{\lambda}^{(k)}$ requires to solve two differential problems in each subdomain.

We can compute a Cholesky or LU factorization of both A_{11} and A_{22} off-line, before the iterations start, and then solve the associated triangular systems every time we have to compute the matrix-vector product $S_D\boldsymbol{\lambda}^{(k)}$, otherwise we can solve each system $A_{ii}\mathbf{u}_i = -B_i\boldsymbol{\lambda}_i$ (and the corresponding dual problem) by the Preconditioned Conjugate Gradient (PCG) method (or one variants of its for non-symmetric problems). Low-order FEM-preconditioners can be used when SEM-NI discretization is adopted. It is well known (see, e.g. [22, 24]) that such preconditioners cluster the eigenvalues of SEM-NI matrices independently of the discretization.

Remark 4.1 (Additive and multiplicative versions)
The solution of the primal state problems (similar considerations hold for the duals) can be performed either concurrently or sequentially, yielding either *additive* or *multiplicative* versions of the algorithm. More precisely, the form (44) corresponds to the additive version, while the multiplicative one can be achieved by eliminating either the variable $\boldsymbol{\lambda}_1$ or $\boldsymbol{\lambda}_2$ from (44).

Remark 4.2
Instead of solving the Schur-complement system (46), it is possible to solve the discrete optimality system (44) simultaneously for the primal states, dual states and controls, using the so-called *one-shot* (or *all-at-once*) approach analyzed in [26, 27, 28, 29].

Remark 4.3
In principle the discretizations to be used in Ω_1 and Ω_2 may be totally unrelated, so that either the polynomial degrees p_i and/or the mesh size inside each subdomain Ω_i may differ one another. This implies that the restrictions to the overlapping region Ω_{12} of the partitions $\mathcal{T}_1$ and $\mathcal{T}_2$ may not match on Ω_{12} and the set up of an intergrid interpolation operator (from either $\mathcal{T}_1$ to $\mathcal{T}_2$ or *viceversa*) is needed to compute both the terms $(C_1^0\mathbf{u}_1 - C_2^0\mathbf{u}_2)$ and $(C_1^{\Gamma_1}\boldsymbol{\lambda}_1 - C_2^{\Gamma_2}\boldsymbol{\lambda}_2)$. This step can be expensive if the overlapping region is wide and the meshes are very fine in Ω_{12}.
In our numerical tests, only matching meshes on the overlap will be taken into account when the minimization of both cost functionals (12) and (13) are performed.
Different conclusions can be carried out when the minimization of the cost functional (14) is considered since, in such case, the interpolation is required only on the interface Γ_i, as we can see the in next Section.

4.4. *Interface observation. Dirichlet controls*

In order to write the algebraic form of OS (20) we introduce the following new matrices, for $i = 1, 2$ and $j = 3 - i$:

- T_{ij} is the matrix that interpolates the trace of u_{j,δ_j} on $\mathsf{M}_i \cap \Gamma_i$ (obviously, $T_{ii}\mathbf{u}_i = \boldsymbol{\lambda}_i$);
- $M_i^{\Gamma_i}$ is the $(d-1)$-dimensional mass matrix associated to interface Γ_i,

and we set

$$T = \begin{bmatrix} 0 & T_{12} \\ T_{21} & 0 \end{bmatrix}, \quad M^\Gamma = \begin{bmatrix} M_1^{\Gamma_1} & 0 \\ 0 & M_2^{\Gamma_2} \end{bmatrix}. \tag{47}$$

Recalling the definitions given in (43), the algebraic form of (20) reads

$$\underbrace{\begin{bmatrix} A & 0 & B \\ -BT & A & B \\ -M^\Gamma T & M^\Gamma T & M^\Gamma \end{bmatrix}}_{G_\Gamma} \underbrace{\begin{bmatrix} \mathbf{u} \\ \mathbf{p} \\ \boldsymbol{\lambda} \end{bmatrix}}_{\mathbf{x}} = \underbrace{\begin{bmatrix} \mathbf{f} \\ \mathbf{0} \\ \mathbf{0} \end{bmatrix}}_{\mathbf{b}}. \tag{48}$$

Interpolation matrices T_{ij} depend on both meshes and overlap decomposition and the product $T_{ij}\mathbf{u}_j$ (for $i \neq j$) requires a-priori $\mathcal{O}(N_{\Omega_j}^0 \cdot N_{\Gamma_i})$ floating-point operations. Nevertheless, because of the local support of Lagrange basis functions, the computation of the matrix-vector product $T_{ij}\mathbf{u}_j$ involves only those elements of $\mathcal{T}_j \cap \Omega_j$ whose intersection with the interface Γ_i is non-empty.

Remark 4.4 (Non-matching grids)
The OS (20) offers the advantage of using only the trace of $(u_1^{\lambda_1,f} - u_2^{\lambda_2,f})$ on Γ_i instead of the distributed function $(u_1^{\lambda_1,f} - u_2^{\lambda_2,f})$ in Ω_{12}. Thus, if we use totally unrelated meshes in Ω_1 and Ω_2, the interpolation of u_i on Γ_j (with $i \neq j$) is bounded to the sole elements $T \in \mathcal{T}_i : \ T \cap \Gamma_j \neq \emptyset$.

By introducing the Schur-complement matrix $S_{D\Gamma}$ of G_Γ with respect to the control variable $\boldsymbol{\lambda}$

$$S_{D\Gamma} = M^\Gamma \left(I - \begin{bmatrix} -T & T \end{bmatrix} \begin{bmatrix} A & 0 \\ -BT & A \end{bmatrix}^{-1} \begin{bmatrix} B \\ B \end{bmatrix} \right) = M^\Gamma (I - (TA^{-1}B)^2) \tag{49}$$

and the vector

$$\boldsymbol{\psi}_{D\Gamma} = M^\Gamma (I - TA^{-1}B) TA^{-1}\mathbf{f}$$

the Schur-complement system associated to OS (48) reads

$$S_{D\Gamma}\boldsymbol{\lambda} = \boldsymbol{\psi}_{D\Gamma} \tag{50}$$

and it is the discrete counterpart of the equation $(20)_3$.

Remark 4.5 (Preconditioning of (50))
Since the mass matrix M^Γ is not singular, we can left-multiply the last row of (48), or equivalently both sides of (49), by $(M^\Gamma)^{-1}$. This operation is in fact a preconditioning step of system (50) by the matrix M^Γ.

In the case of $\mathbb{P}_1$-FEM the elimination of M^Γ does not produce benefits, on the contrary, when $\mathbb{Q}_p$ approximation is used on Legendre-Gauss-Lobatto nodes, the condition number of $S_{D\Gamma}$ reduces by a factor p^{d-1}. We refer to [15] for a detailed analysis of the conditioning of the Schur complement systems (46) and (50).

Given the array $\boldsymbol{\lambda}^{(k)}$ at the $k-$th iteration of Bi-CGStab, the matrix vector product $\boldsymbol{\chi}^{(k)} = S_{D\Gamma}\boldsymbol{\lambda}^{(k)}$ is performed by the following algorithm.

Algorithm 4.3 (Schur-complement evaluation)
Interface observation - Dirichlet controls. Given $\boldsymbol{\lambda}^{(k)}$, compute $\boldsymbol{\chi}^{(k)} = S_{D\Gamma}\boldsymbol{\lambda}^{(k)}$.

1. solve $A_{ii}\mathbf{u}_i^{(k)} = -B_i\boldsymbol{\lambda}_i^{(k)}$ for $i = 1, 2$, i.e. use $\boldsymbol{\lambda}_i^{(k)}$ as Dirichlet data on the interfaces Γ_i and $F_i = 0$ to solve primal states problems;
2. compute $\mathbf{t}_1^{(k)} = T_{12}\mathbf{u}_2^{(k)}$ and $\mathbf{t}_2^{(k)} = T_{21}\mathbf{u}_1^{(k)}$, i.e. the discrete trace of u_1 on $\mathsf{M}_2 \cap \Gamma_2$ and that of u_2 on $\mathsf{M}_1 \cap \Gamma_1$ by interpolation matrices;
3. solve $A_{ii}\mathbf{p}_i^{(k)} = -B_i(\boldsymbol{\lambda}_i^{(k)} - \mathbf{t}_j^{(k)})$ with $j = 3 - i$, i.e., solve the dual state problems;
4. compute

$$\boldsymbol{\chi}^{(k)} = \begin{bmatrix} \boldsymbol{\lambda}_1^{(k)} - T_{12}\mathbf{u}_2^{(k)} + T_{12}\mathbf{p}_2^{(k)} \\ T_{21}\mathbf{u}_1^{(k)} - \boldsymbol{\lambda}_2^{(k)} + T_{21}\mathbf{p}_1^{(k)} \end{bmatrix}.$$

The computation of $\boldsymbol{\psi}_{D\Gamma}$ is performed similarly:

Algorithm 4.4 ($\boldsymbol{\psi}_{D\Gamma}$ evaluation)
Interface observation - Dirichlet controls. Given $\mathbf{f}$, compute $\boldsymbol{\psi}_{D\Gamma}$

1. solve $A\mathbf{u}^f = \mathbf{f}$, i.e. use null Dirichlet data on the interfaces Γ_i and F_i as in (18) to solve primal states problems and find $\mathbf{u}^f$;
2. compute $\mathbf{t}_1 = T_{12}\mathbf{u}_2^f$ and $\mathbf{t}_2 = T_{21}\mathbf{u}_1^f$, i.e. the discrete trace of u_1 on $\mathsf{M}_2 \cap \Gamma_2$ and that of u_2 on $\mathsf{M}_1 \cap \Gamma_1$ by interpolation matrices;
3. solve $A_{ii}\mathbf{p}_i^f = B_i\mathbf{t}_j$, i.e., solve the dual state problems (with $j = 3 - i$);
4. compute

$$\boldsymbol{\psi}_{D\Gamma} = \begin{bmatrix} -T_{12}\mathbf{u}_2^f + T_{12}\mathbf{p}_2^f \\ T_{21}\mathbf{u}_1^f + T_{21}\mathbf{p}_1^f \end{bmatrix}.$$

As for distributed observation, also in this case the primal state problems (and similarly the duals) can be solved either simultaneously (additive form) or sequentially (multiplicative form).

4.5. *Distributed observation. Robin controls.*

Let us consider now the OS (21), all definitions given in Section 4.3, and we define some new matrices:

- the restriction matrices $R_i \in \mathbb{R}^{N_{\Gamma_i} \times N_{\Omega_i^0}}$ made of 0,1 implementing the restriction map from M_i^0 to M_{Γ_i};

- matrices associated to state equations in $(21)_1$ and $(21)_2$, i.e. $A_{ii}^\beta = A_{ii} + \beta R_i^T M^{\Gamma_i}$;

and

$$A^\beta = \begin{bmatrix} A_{11}^\beta & 0 \\ 0 & A_{22}^\beta \end{bmatrix}, \; R = \begin{bmatrix} R_1 & 0 \\ 0 & R_2 \end{bmatrix}.$$

The algebraic form of OS 21) reads:

$$\begin{bmatrix} A^\beta & 0 & -R^T \\ C & (A^\beta)^T & 0 \\ 0 & M^\Gamma R & 0 \end{bmatrix} \begin{bmatrix} \mathbf{u} \\ \mathbf{p} \\ \boldsymbol{\lambda} \end{bmatrix} = \begin{bmatrix} \mathbf{f} \\ \mathbf{0} \\ \mathbf{0} \end{bmatrix}. \tag{51}$$

Also in this case we can write the Schur-complement system $S_R\boldsymbol{\lambda} = \boldsymbol{\chi}$ of (21) with respect to the control variable, but now

$$S_R = -\begin{bmatrix} 0 & M^\Gamma R \end{bmatrix} \begin{bmatrix} A^\beta & 0 \\ C & (A^\beta)^T \end{bmatrix}^{-1} \begin{bmatrix} -R^T \\ 0 \end{bmatrix} = -M^\Gamma R (A^\beta)^{-T} C (A^\beta)^{-1} R^T \tag{52}$$

and

$$\boldsymbol{\psi}_R = M^\Gamma R (A^\beta)^{-T} C (A^\beta)^{-1} \mathbf{f}.$$

At the kth Bi-CGStab iteration, if $\boldsymbol{\lambda}^{(k)}$ is a known array, the computation of the matrix-vector product $\boldsymbol{\chi}^{(k)} = S_R\boldsymbol{\lambda}^{(k)}$ with S_R defined in (52) is performed by the following algorithm which, in fact, reflects the three steps of the OS (21).

Algorithm 4.5 (Schur-complement evaluation)
Distributed observation - Robin controls. Given $\boldsymbol{\lambda}^{(k)}$, compute $\boldsymbol{\chi}^{(k)} = S_R\boldsymbol{\lambda}^{(k)}$

1. solve $A^\beta \mathbf{u}^{(k)} = R^T\boldsymbol{\lambda}^{(k)}$, i.e. use $\boldsymbol{\lambda}^{(k)}$ as Robin data on the interfaces Γ_i and null functions F_i to solve primal states problems and find $\mathbf{u}^{(k)}$;
2. solve $(A^\beta)^T \mathbf{p}^{(k)} = C\mathbf{u}^{(k)}$, i.e., use $\mathbf{u}^{(k)}$ to assemble the right hand side for the dual state problems and find $\mathbf{p}^{(k)}$;
3. compute $\boldsymbol{\chi}^{(k)} = -M^\Gamma R\mathbf{p}^{(k)}$, i.e. compute the weak trace of $p_{i,\delta}^{(k)}$ at the interfaces Γ_i.

The right hand side $\boldsymbol{\psi}_R$ is computed by a similar algorithm:

Algorithm 4.6 ($\boldsymbol{\psi}_R$ evaluation)
Distributed observation - Robin controls. Given $\mathbf{f}$, compute $\boldsymbol{\psi}_R$

1. solve $A^\beta \mathbf{u}^f = \mathbf{f}$, i.e. use null Robin data on the interfaces Γ_i and F_i as in (18) to solve primal states problems and find $\mathbf{u}^f$;
2. solve $(A^\beta)^T \mathbf{p}^f = C\mathbf{u}^f$ with null Robin data on the interfaces;
3. compute $\boldsymbol{\psi}_R = M^\Gamma R\mathbf{p}^f$.

4.6. Interface observation. Robin controls

Let us consider now the OS (22), by proceeding as in previous Sections, its algebraic form reads:

$$\begin{bmatrix} A^\beta & 0 & -R^T \\ M^\Gamma(R-T) & A^\beta & 0 \\ M^\Gamma(R-T) & M^\Gamma T & 0 \end{bmatrix} \begin{bmatrix} \mathbf{u} \\ \mathbf{p} \\ \boldsymbol{\lambda} \end{bmatrix} = \begin{bmatrix} \mathbf{f} \\ \mathbf{0} \\ \mathbf{0} \end{bmatrix}. \tag{53}$$

The Schur-complement matrix is now

$$S_{R\Gamma} = M^\Gamma (I - T(A^\beta)^{-1} M^\Gamma)(R-T)(A^\beta)^{-1} R^T \tag{54}$$

while the right hand side is

$$\boldsymbol{\psi}_{R\Gamma} = -M^\Gamma (I - T(A^\beta)^{-1} M^\Gamma)(R-T)(A^\beta)^{-1} \mathbf{f}.$$

The corresponding algorithm to perform the matrix-vector product reads as follows.

Algorithm 4.7 (Schur-complement evaluation)
Interface observation - Robin controls. Given $\boldsymbol{\lambda}^{(k)}$, compute $\boldsymbol{\chi}^{(k)} = S_{R\Gamma}\boldsymbol{\lambda}^{(k)}$

1. solve $A^\beta \mathbf{u}^{(k)} = R^T \boldsymbol{\lambda}^{(k)}$, i.e. use $\boldsymbol{\lambda}^{(k)}$ as Robin data on the interfaces Γ_i and null functions F_i to solve primal states problems and find $\mathbf{u}^{(k)}$;
2. compute $\mathbf{t}_1^{(k)} = T_{12}\mathbf{u}_2^{(k)}$ and $\mathbf{t}_2^{(k)} = T_{21}\mathbf{u}_1^{(k)}$, i.e. the discrete trace of u_1 on $\mathsf{M}_2 \cap \Gamma_2$ and that of u_2 on $\mathsf{M}_1 \cap \Gamma_1$ by interpolation matrices, and the restrictions of u_i to Γ_i by matrices R_i;
3. solve $A_{ii}\mathbf{p}_i^{(k)} = M_i^{\Gamma_i}(R_i\mathbf{u}_i^{(k)} - \mathbf{t}_j^{(k)})$ with $j = 3 - i$, i.e., solve the dual state problems;
4. compute

$$\boldsymbol{\chi}^{(k)} = \begin{bmatrix} R_1\mathbf{u}_1^{(k)} - T_{12}\mathbf{u}_2^{(k)} + T_{12}\mathbf{p}_2^{(k)} \\ T_{21}\mathbf{u}_1^{(k)} - R_2\mathbf{u}_2^{(k)} + T_{21}\mathbf{p}_1^{(k)} \end{bmatrix}.$$

The right hand side $\boldsymbol{\psi}$ is computed by a similar algorithm:

Algorithm 4.8 ($\boldsymbol{\psi}$ evaluation)
Distributed observation - Robin controls. Given $\mathbf{f}$, compute $\boldsymbol{\psi}_{R\Gamma}$

1. solve $A^\beta \mathbf{u}^f = \mathbf{f}$, i.e. use null Robin data on the interfaces Γ_i and F_i as in (18) to solve primal states problems and find $\mathbf{u}^f$;
2. compute $\mathbf{t}_1 = T_{12}\mathbf{u}_2^f$ and $\mathbf{t}_2 = T_{21}\mathbf{u}_1^f$, i.e. the discrete trace of u_1^f on $\mathsf{M}_2 \cap \Gamma_2$ and that of u_2^f on $\mathsf{M}_1 \cap \Gamma_1$ by interpolation matrices, and the restrictions of u_i^f to Γ_i by matrices R_i;
3. solve $A_{ii}\mathbf{p}_i^f = M_i^{\Gamma_i}(R_i\mathbf{u}_i^f - \mathbf{t}_j)$ with $j = 3 - i$, i.e., solve the dual state problems;
4. compute

$$\boldsymbol{\psi}_{R\Gamma} = -\begin{bmatrix} R_1\mathbf{u}_1^f - T_{12}\mathbf{u}_2^f + T_{12}\mathbf{p}_2^f \\ T_{21}\mathbf{u}_1^f - R_2\mathbf{u}_2^f + T_{21}\mathbf{p}_1^f \end{bmatrix}.$$

5. NUMERICAL RESULTS

In this section we compare the ICDD methods presented above, with either Dirichlet and Robin controls for two dimensional domains, versus the discretization parameters h and p and the overlap thickness $\delta_{12} = \mathrm{dist}(\Gamma_1, \Gamma_2)$.

Then we consider jumping coefficients and discuss the robustness of ICDD methods with interface observation and Dirichlet controls.

Each ICDD method is characterized by the type of controls (Dirichlet or Robin) and the norm chosen for the minimization, thus we introduce the following notations:

Signature	Controls	Observation	Cost functional	OS
J0D	Dir	distributed	J_0 (12)	(19)
J1D	Dir	distributed	J_1 (13)	(19)
JGD	Dir	on interfaces	$J_{0,\Gamma}$ (14)	(20)
J0R	Robin	distributed	J_0 (12)	(21)
J1R	Robin	distributed	J_1 (13)	(21)
JGR	Robin	on interfaces	$J_{0,\Gamma}$ (14)	(22)

Only 2D geometries are considered here.

Numerical results refer to discretization with either simplicial meshes and $p = 1$ (identified by the classical notation $\mathbb{P}_1$) or quad meshes and $p \geq 1$ (identified by $\mathbb{Q}_p$).

In general the partitions $\mathcal{T}_i$ in each Ω_i are uniform and h denotes the global size of the mesh, but we can also use finer mesh on the overlap, especially when jumping coefficients generate internal layers. More precisely, when non-matching grids are used, the meshes are uniform and regular in each Ω_i and in the whole domain. When we work with matching grids we can use either uniform and non-uniform meshes: with finer grids in Ω_{12} and coarser grids in $\Omega \setminus \Omega_{12}$.

When the observation of the optimization problem is distributed, the simpler way of working consists in considering matching grids on the overlap Ω_{12}, in order to avoid interpolation processes

Table I. *Test case #1*. The number of iterations reported in Figs. 3–4 obeys the law $it \simeq ch^q p^s$

	J0D	J1D	JGD	J0R	J1R	JGR
q for $\mathbb{P}_1$	-0.25	-0.5	0	-1	-0.5	-0.25
q for $\mathbb{Q}_p$	0.4	0.6	0	1.5	1	0.4
s for $\mathbb{Q}_p$	-0.3	0.2	0	-1	-0.8	-0.4

between the state solutions on the whole overlap. On the contrary, when the observation is bounded to interfaces, we consider both matching and non-matching grids in Ω_{12} (see Remarks 4.3 and 4.4).

The efficiency of each method is measured in terms of Bi-CGStab iterations to solve the Schur complement system associated to its OS.

As noticed in Remark 4.5, the Schur complement system is preconditioned by the mass matrix on the interfaces. The computational cost of one Bi-CGStab iteration is of 4 boundary value problems on each subdomain and it is independent of the specific type of ICDD method used.

The tolerance of the stopping test is chosen equal to $\epsilon = 10^{-9}$.

5.1. Test case #1. Homogeneous elliptic coupling with self-adjoint operator L

Let us consider the elliptic problem (2) and set $\nu = 1$, $\gamma = 1$, $\mathbf{b} = (0,0)$ and Dirichlet boundary conditions on $\partial\Omega$. The functions f and ϕ_D are defined so that the exact solution of the differential problem (2) is $u(x,y) = \sin(\pi xy) + 1$.

The domain $\Omega = (0,1)^2$ is decomposed in two subdomains of the same size, the interfaces Γ_1 and Γ_2 are parallel to the vertical axis and symmetric with respect to the line $x = 0.5$, δ_{12} is the thickness of the overlap. In this test case we consider matching grids in Ω_{12}.

At first we analyze the convergence rate of ICDD methods with respect to the discretization parameters p and h.

In Figure 3 (left) the number of iterations of all ICDD methods is shown versus the mesh size h for $\mathbb{P}_1$ discretization. The overlap thickness is $\delta_{12} = 1/10$.

In Figure 3 (right) the number of iterations of all ICDD methods is shown versus the polynomial degree p for $\mathbb{Q}_p$ discretization. The overlap thickness and the mesh-size are fixed, more precisely $\delta_{12} = 1/10$ and $h = 1/10$.

In Figure 4 the number of iterations of all ICDD methods is shown versus the mesh size h of $\mathbb{Q}_p$ discretization, with $p = 4$. The overlap thickness is $\delta_{12} = 1/10$.

We see that JGD is the sole method whose convergence rate is independent of the discretization parameters, while the number of Bi-CGStab iterations of the other methods grows for $p \nearrow$ and $h \searrow$. For each stage, we have computed a least-squares fit of a law like $it \simeq ch^q p^s$, for h and p in the range of the values indicated in Figures 3–4 and c a positive constant independent of both p and h. The estimated values for q and s are shown in Table I.

We notice that J0D and J1R behave similarly and that the worst method is J0R.

Now we fix the discretization and analyze the convergence rate of ICDD methods with respect to the overlap thickness δ_{12}, more precisely when $\delta_{12} \to 0$. To perform this analysis we can proceed in different ways.

1. by fixing the mesh (i.e. both h and p) on the whole domain and setting $\delta_{12} = Ch$ where $C = \ldots, 3, 2, 1$. (in this case δ_{12} is bounded below by the mesh size h). See Figure 5;
2. by fixing p, by taking uniform h in the whole domain Ω and choosing $\delta_{12} = h$, in this case both $\delta_{12} \to 0$ and $h \to 0$. See Figure 6 (left);
3. only for non-matching grids, by moving δ_{12} to zero independently of the mesh. In this case we fix p and the number of elements in each subdomain Ω_i; the mesh is uniform in each Ω_i, but obviously the mesh size h slowly changes and it grows up when $\delta_{12} \searrow$. In this case we analyze only ICDD methods with interface observation (JGD and JGR) in order to avoid interpolation of the state solutions on the whole overlap Ω_{12}. See Figures 6– 7.

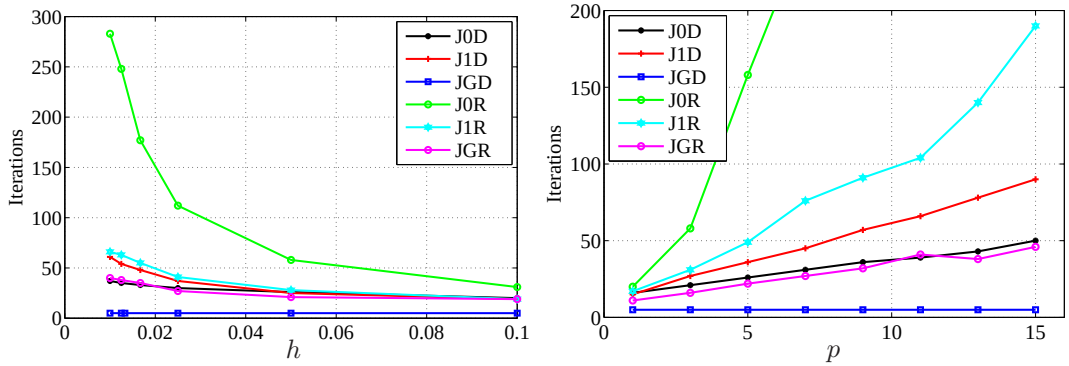

Figure 3. *Test case #1.* Iterations versus the mesh size h. $\mathbb{P}_1$ discretization, $\delta_{12} = 1/10$ (at left). Iterations versus the polynomial degree p. $\mathbb{Q}_p$ discretization, $\delta_{12} = 1/10$, the mesh size is $h = 1/10$ (at right)

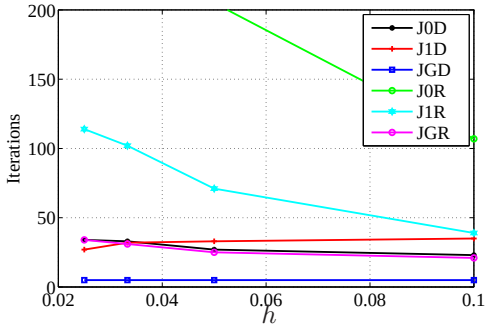

Figure 4. *Test case #1.* Iterations versus the mesh size h. $\mathbb{Q}_p$ discretization with $p = 4$, $\delta_{12} = 1/10$

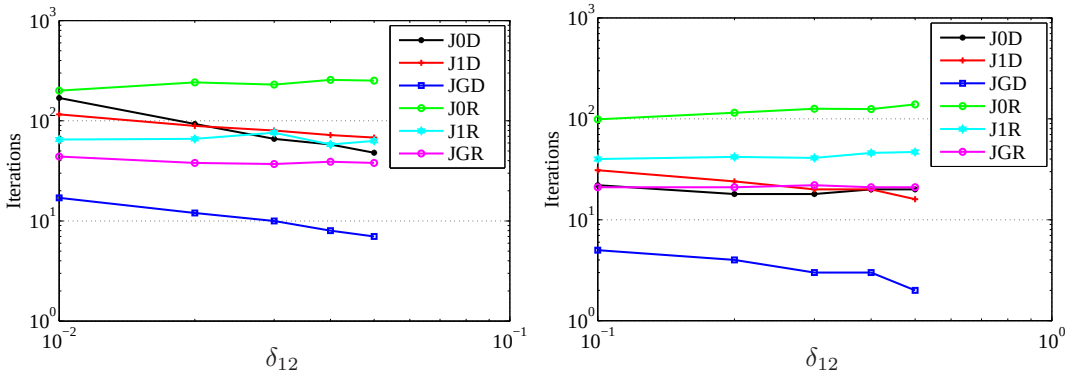

Figure 5. *Test case #1.* Iterations versus the overlap thickness $\delta_{12} \geq h$. $\mathbb{P}_1$ discretization with $h = 1/100$ (at left). Iterations versus the overlap thickness $\delta_{12} \geq h$. $\mathbb{Q}_p$ discretization with $p = 4$ and $h = 1/10$ (at right)

The behaviour of ICDD methods w.r.t. δ_{12} depends on the way δ_{12} and h are related one another, as said in the previous description. In all cases we look for an exponent r so that $it \simeq c\delta_{12}^r$, with $c > 0$ independent of δ_{12}.

When $\delta_{12} = Ch$, h is fixed and $C = 1, \ldots, 5$ (results of Fig. 5), r is given in Table II (top), while when $\delta_{12} = h$ (results of Fig. 6 (left)), r is given in Table II (bottom).

Finally, we consider JGD and JGR with non-matching grids on the overlap and $\delta_{12} \to 0$ independently of h. As we can see in Fig. 6 (right), JGD and JGR show specular behaviors, more

Table II. *Test case #1.* The number of iterations of Figs. 5 and 6-left behaves like $it \simeq c\delta_{12}^{r}$

Fig. 5	J0D	J1D	JGD	J0R	J1R	JGR
r for $\mathbb{P}_1$	-0.8	-0.3	-0.5	0.1	0	0
r for $\mathbb{Q}_p$	0	-0.4	-0.5	0.2	0	0
Fig. 6-left	J0D	J1D	JGD	J0R	J1R	JGR
r for $\mathbb{P}_1$	-1	-1	-0.5	-1	-0.5	-0.4

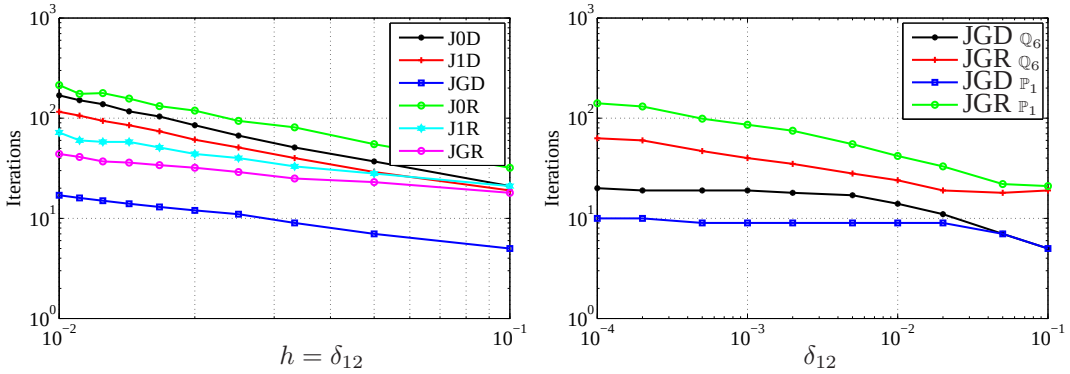

Figure 6. *Test case #1.* Iterations versus $\delta_{12} = h$. $\mathbb{P}_1$ discretization (at left). Non-matching grids on the overlap. $h = 1/5$ for $\mathbb{Q}_6$, $h = 1/20$ for $\mathbb{P}_1$ (at right)

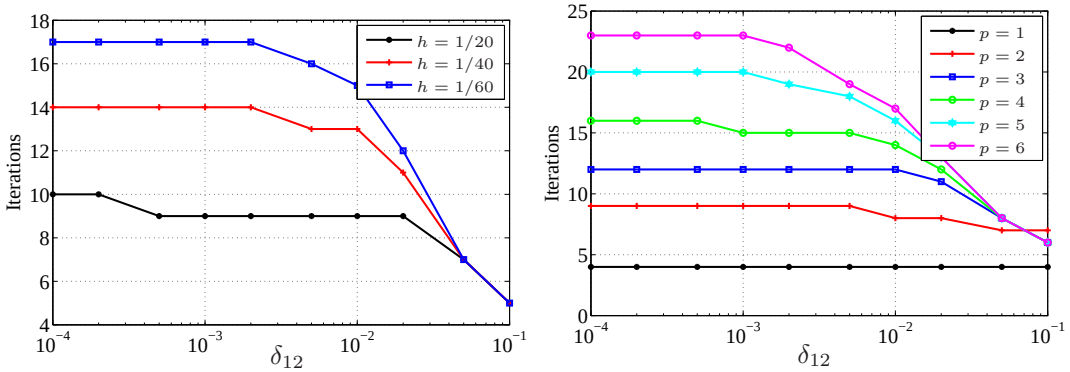

Figure 7. *Test case #1.* Iterations of JGD versus δ_{12}. $\mathbb{P}_1$ discretization, non-matching grids on the overlap (at left). $\mathbb{Q}_p$ discretization with $h = 1/5$, non-matching grids on the overlap (at right)

precisely the number of iterations of JGD slightly grows when δ_{12} decreases and it is large, while it is independent of δ_{12} when δ_{12} is smaller than a value $\overline{\delta}$ that depends on the discretization (either $\mathbb{P}_1$ or $\mathbb{Q}_6$). On the contrary, the number of iteration of JGR is fixed for large δ_{12} and than it grows when $\delta_{12} \to 0$. In both cases, the behavior for large δ_{12}, i.e. $\delta_{12} \geq h$ is the one shown in Figs. 5–6.

In order to better understand the behavior of the methods for very small δ_{12}, we compare the iterations of JGD for several values of h and p in Fig. 7. Numerical results show that

$$it_{JGD} \simeq \min\left\{c_1 p h^{-1/2}, c_2 \delta_{12}^{-1/2}\right\}, \tag{55}$$

with c_1, c_2 positive constants independent of $h,\ p,\ \delta_{12}$.

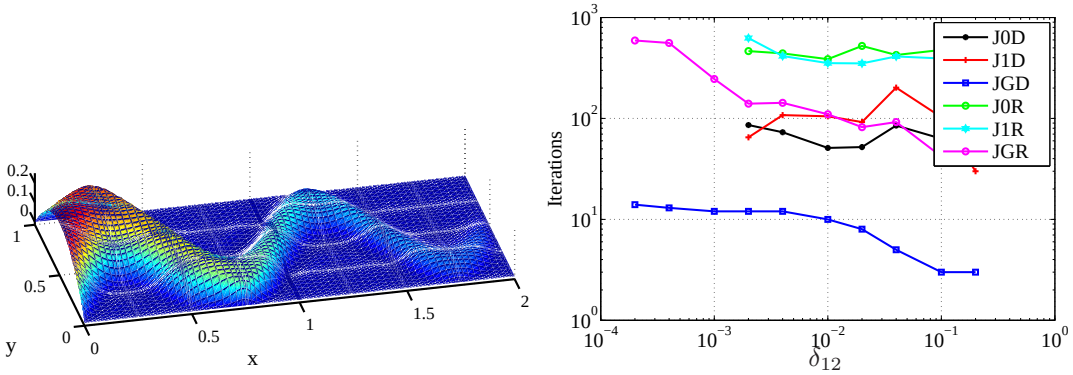

Figure 8. *Test case #2.* Numerical solution obtained with $\mathbb{Q}_p$ with $p = 6$ and 5×5 quad elements in each subdomain. The convergence is achieved in 8 iterations (at left). Iterations versus δ_{12} (at right)

5.2. Test case #2. Homogeneous coupling, advection–diffusion operator

We consider now the advection diffusion problem (2) in $\Omega = (0, 2) \times (0, 1)$ with $\nu = 10^{-4}$, $\mathbf{b} = [1, 2\cos(2\pi x)]^t$, $\gamma = 1$, $f = 0$ and Dirichlet boundary conditions $\phi_D = y(1 - y)$ on the left vertical side of the domain and $\phi_D = 0$ otherwise.

We apply Galerkin Least Squares (GaLS) stabilization techniques (see [30, 31]) to hp-FEM, more precisely we discretize the differential problems by $\mathbb{Q}_p$ with $p = 6$ and 5×5 quad elements in each subdomain. When the methods with distributed observation (i.e. J0D, J1D, J0R, J1R) are considered the two meshes match on the overlap. On the contrary, non-matching meshes are used for both JGD and JGR. The numerical solution is shown in Figure 8 (left).

We split the domain in two symmetric subdomains with respect to the line $x = 1$ and we measure the convergence rate of various ICDD methods. For this test case we only report the number of iterations versus the overlap thickness (see Fig. 8 (right)). The behaviour of the various methods with respect to the discretization parameters is as in the test case #1without advection (see Figs. 3–4).

As we can deduce from Figure 8 (right), we observe that the most efficient method is JGD, also in presence of non-null advective fields.

5.3. Test case #3. Homogeneous coupling with jumping viscosity.

In this test case we consider only the JGD method, the most efficient one among the six methods presented in the previous sections, and we test its robustness with respect to jumps discontinuities of the elliptic coefficient ν.

We take $\Omega = (0, 1)^2$ and we decompose it in more than two subdomains, as described in Remark 2.1.

At first we consider discontinuous viscosity ν as on a chessboard with squares of size 1/5, ν assumes the value 10 in the white squares and the value α (as precised in Table III) in the black ones, while the reaction coefficient is $\gamma = 1$. Then we consider a random mix of values for ν as defined in Figure 9 (left).

In both cases we take $\mathbf{b} = [0, 0]^t$, $f = 1$ and homogeneous Dirichlet boundary conditions.

The computational domain is decomposed in 5×5 equal overlapping subdomains with overlap thickness $\delta_{12} = 0.01$ (equal to 1% of the side of Ω), $\mathbb{Q}_p$ discretization is considered in each subdomain with $p = 12$ and 3×3 non-uniform quad elements.

The size of the overlap is responsible in general for the convergence rate of the Bi-CGStab iterations and, in the case of discontinuous coefficient, also for the accuracy of the approximation. More precisely, if the jump of the coefficient is very large, the high variation of the solution is correctly captured without oscillations only if the discretization is fine enough in a small region around the jump. We can achieve good results, e.g., by using a very small overlap, then considering

Table III. *Test case #3* Iterations count and infimum of the cost functional $J_{0,\Gamma}$ for the *chessboard* and *random mix* configurations

α	iterations	$\inf J_{0,\Gamma}$
10^{-5}	16	$3 \cdot 10^{-22}$
10^{-3}	9	$1 \cdot 10^{-26}$
10^{-1}	13	$7 \cdot 10^{-31}$
10^{3}	11	$7 \cdot 10^{-35}$
10^{5}	8	$4 \cdot 10^{-34}$
random	10	$2 \cdot 10^{-19}$

1	10^{4}	1	10^{-5}	1
10^{-2}	10	10^{-2}	10	10^{2}
10^{-6}	10^{-3}	10^{-6}	10^{3}	10^{6}
10	10^{-1}	10^{2}	10^{-2}	10
10^{3}	10^{-4}	10^{3}	10^{4}	10^{-3}

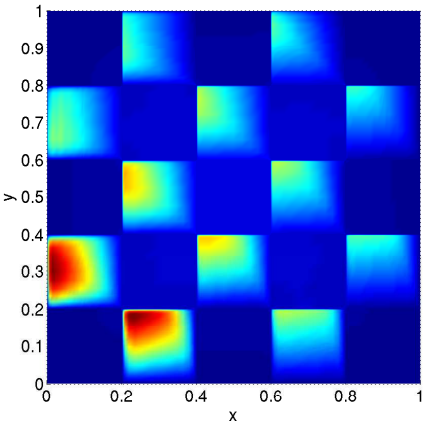

Figure 9. *Test case #3* Values of the viscosity ν in Ω for the random mix case (at left). Numerical solution of advection-diffusion problem with $\nu = 10$ or $\nu = 10^{-3}$ as on a 5×5 chessboard and $\mathbf{b} = [-y, x]^t$. The solution is computed by JGD and $\mathbb{Q}_p$ with $p = 12$ and 3×3 quad elements in each subdomain. The convergence is achieved in 10 iterations (at right)

matching meshes and discretizing the overlap with one spectral element (along the direction across the jump) and by using a moderately large value of the polynomial degree p. Otherwise we can use a generous overlap in spite of adopting a higher polynomial degree p. On one hand, the smaller the overlap thickness, the slower the convergence rate to the minimum point. On the other hand, the larger the polynomial degree p, the more expensive the solution of the boundary value problems inside each subdomain. Therefore, a careful tuning of the discretization parameters is in order to minimize the computational costs without compromising accuracy or stability.

In Table III we report the iterations count and the infimum of the cost functional $J_{0,\Gamma}$ obtained at convergence, for different values of the parameter α. The iterations count refers to Bi-CGStab, called here to solve the Schur complement system (48). The stopping test is satisfied when the norm of the residual is reduced up to 10^{-12}.

The results show that the convergence rate of JGD to the solution of the minimum problem (14) is independent of the jumps of the coefficients.

At last we consider again the chessboard configuration of the viscosity with $\nu = 10$ in the white squares and $\nu = 10^{-3}$ on the black ones, but now we take non-null advective field, precisely $\mathbf{b} = [-y, x]^t$.

Again, we set $\gamma = 1$, $f = 1$ and homogeneous Dirichlet boundary conditions. The discretization is the same used for the case with null $\mathbf{b}$.

The numerical solution, computed with stabilized Galerkin Least Squares hp-FEM, is shown in Figure 9 (right).

Table IV. *Test case #3*, advection-diffusion problem. Iteration counts of JGD and infimum of the cost functional $J_{0,\Gamma}$ versus the overlap thickness

δ_{12}	iterations	$\inf J_{0,\Gamma}$
$1 \cdot 10^{-1}$	9	$3.50 \cdot 10^{-26}$
$5 \cdot 10^{-2}$	9	$7.40 \cdot 10^{-27}$
$2 \cdot 10^{-2}$	10	$1.58 \cdot 10^{-26}$
$1 \cdot 10^{-2}$	10	$2.96 \cdot 10^{-26}$
$5 \cdot 10^{-3}$	11	$6.99 \cdot 10^{-27}$
$2 \cdot 10^{-3}$	12	$2.98 \cdot 10^{-27}$
$1 \cdot 10^{-3}$	12	$8.70 \cdot 10^{-28}$

Table V. *Test case #4*. Iterations count of JGD for fixed $h = 1/7$, $\delta_{12} = 0.01$ and $\nu = 10^{-3}$ (at left). Iterations count of JGD for fixed $p = 2$, $\delta_{12} = 0.1$ and $\nu = 10^{-3}$ (at right)

p	1	2	3	4	5	6	7	8
#it	3	3	3	3	3	3	3	3

h	1/10	1/20	1/30	1/40	1/50
#it	3	2	1	1	1

Table VI. *Test case #4*. Iterations count of JGD for fixed $p = 4$, $h = 1/16$ and $\nu = 10^{-3}$

δ_{12}	0.1	0.05	0.02	0.01	0.005	0.002	0.001
#it(matching grids)	3	2	2	3	5	9	13
#it(non-matching grids)	1	2	4	3	5	6	6

We have analyzed the number of iterations of JGD and the infimum of $J_{0,\Gamma}$ attained at convergence with respect to the overlap thickness δ_{12}, the results are shown in Table IV and show that the method behaves as with self-adjoint elliptic operators (see Test case #1).

Even if the theoretical analysis of convergence rate of ICDD methods is in progress, we can state that JGD is optimal with respect to discretization parameters and it is robust with respect to variations of coefficients for both self-adjoint and advection-diffusion differential elliptic operators.

5.4. Test case #4

We consider again the sole JGD method and we test its robustness in the presence of internal layers, due to low regularity of the advective field $\mathbf{b}$.

We take $\Omega = (0,1)^2$, $\gamma = 1$, $f = 1$, homogeneous Dirichlet boundary conditions and

$$\mathbf{b} = [100 \arctan(|(x-0.5)(y-0.5)|), 10]^t$$

(see Fig. 10 (left)). The viscosity will be specified after.

The computational domain is decomposed in 2 equal overlapping subdomains with overlap thickness δ_{12}, the interfaces are parallel to the axis $x = 0$. The discretization is performed by stabilized (GLS) $\mathbb{Q}_p$ [32].

The numerical solution corresponding to viscosity $\nu = 10^{-6}$ is shown in Fig. 10 (right), it is computed with $p = 8$ and mesh-size $h = 1/16$. The overlap thickness is $\delta_{12} = 0.01$. The convergence of JGD is achieved in 3 iterations up to a tolerance $\epsilon = 10^{-12}$.

Also in this case the convergence rate of JGD is independent of both polynomial degree p and mesh-size h as it is shown in Table V.

We analyze the behavior of JGD also versus the overlap thickness (see Table VI) and the value of the viscosity, that is a constant ranging between 10^{-6} and 1 (see Table VII). In both cases we consider either matching and non-matching grids on the overlap. From Table VII it is evident that the convergence rate of JGD depends on both ν and δ_{12} and, smaller the viscosity greater the convergence rate.

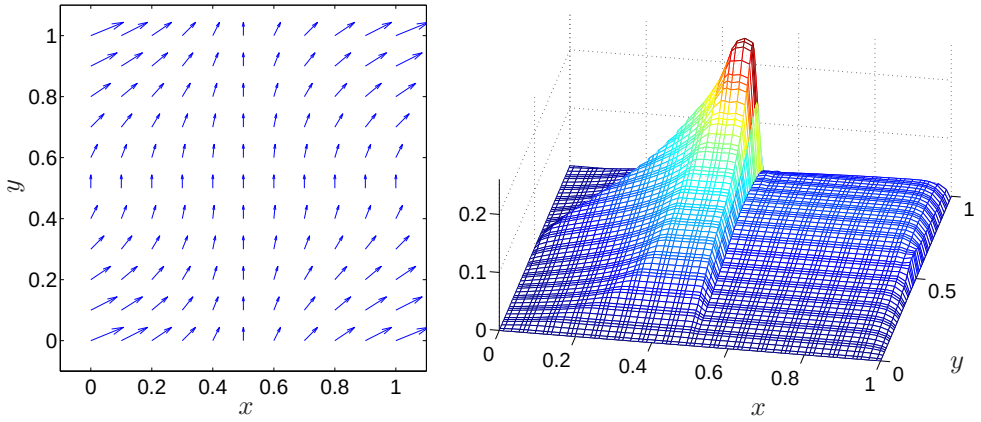

Figure 10. *Test case #4.* Advection field $\mathbf{b}$ (at left). Numerical solution of advection-diffusion problem with viscosity $\nu = 10^{-6}$ obtained by JGD and stabilized $\mathbb{Q}_p$ with $p = 4$, $h = 1/16$ and $\delta_{12} = 0.001$ with non-matching grids (at right)

Table VII. *Test case #4.* Iterations count of JGD for fixed $p = 4$, $h = 1/16$ and $\delta_{12} = 0.001$

	matching grids		non-matching grids	
ν	#it	$\inf J_{0,\Gamma}$	#it	$\inf J_{0,\Gamma}$
1	35	$3 \cdot 10^{-31}$	26	$4 \cdot 10^{-34}$
10^{-1}	36	$1 \cdot 10^{-30}$	25	$6 \cdot 10^{-31}$
10^{-2}	35	$4 \cdot 10^{-30}$	14	$6 \cdot 10^{-31}$
10^{-3}	13	$1 \cdot 10^{-31}$	6	$1 \cdot 10^{-32}$
10^{-4}	5	$1 \cdot 10^{-34}$	3	$4 \cdot 10^{-33}$
10^{-5}	2	$4 \cdot 10^{-34}$	3	$6 \cdot 10^{-29}$
10^{-6}	1	$3 \cdot 10^{-34}$	3	$3 \cdot 10^{-29}$

6. NUMERICAL RESULTS FOR A-AD COUPLING

In this section we report three test cases showing the robustness of ICDD method JGD also for the heterogeneous coupling between Advection and Advection-Diffusion problems.

In the first test case the advective field is parallel to x axis, the computational domain is split in two overlapping subdomains and the interface of the hyperbolic domain has both inflow and outflow parts. The discretization is not uniform on the whole domain, and non-matching grids are considered on the overlap.

In the second test case the vector field is diagonal w.r.t both axis, the computational domain is decomposed in 4 rectangular subdomains, the first one is of "hyperbolic type" (in the sense that there the reduced differential operator is discretized) while the other three subdomains are of "elliptic type". The discretization is adapted to the behaviour of the solution and non-matching grids are used on the overlap regions. The whole interface of the hyperbolic domain is of output type so that the solution inside the hyperbolic domain only depends on external data. The ICDD iterations take into account interactions among the elliptic subdomains.

In the last test case the advective field behaves like a cosine, the computational domain is split in two hyperbolic and two elliptic subdomains as in a chessboard, according to the presence of two layers. In this case the interfaces of both hyperbolic subdomains have inflow and outflow subsets. The meshes used are highly non-conforming on the overlap regions.

We test the robustness of the ICDD method JGD (with interface observation and Dirichlet controls) w.r.t. the variations of the viscosity and of the overlap tichkness.

Table VIII. *Test case #5*. Interfaces setting: smaller the viscosity, wider the hyperbolic domain

ν	x_g	$\delta_{12} \in$
10^{-5}	0.995	$[2.e-5, 2.e-3]$
10^{-4}	0.98	$[2.e-5, 2.e-2]$

ν	x_g	$\delta_{12} \in$
10^{-3}	0.95	$[2.e-5, 2.e-2]$
10^{-2}	0.5	$[2.e-5, 2.e-2]$

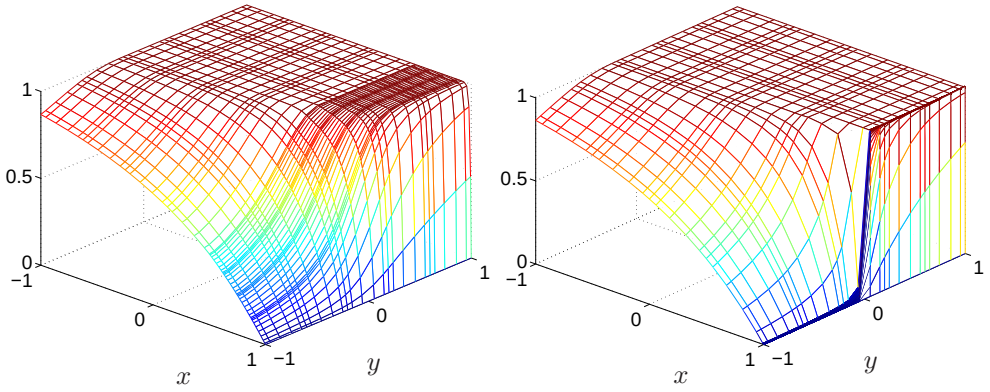

Figure 11. *Test case #5*. Numerical solution for $\nu = 10^{-2}$, the interfaces are parallel to the $y-$ axis and the corresponding abscissa are $x_{1,2} = 0.5 \pm 0.0002$ (at left). Numerical solution for $\nu = 10^{-5}$, the interfaces are parallel to the $y-$ axis and the corresponding abscissa are $x_{1,2} = 0.995 \pm 0.00002$ (at right)

6.1. Test case #5

Let us consider now the heterogeneous coupling described in Section 3 between advection and advection-diffusion differential problems.

Let us set $\Omega = (-1,1)^2$, ν is a small positive constant that will be specified later, $\mathbf{b} = [y,0]^t$, $\gamma = 1$, $f = 1$. If we take constant viscosity ν we are in presence of a convection-dominated problem whose solution features a boundary layer of with $\mathcal{O}(\nu/|\mathbf{b}|)$ (when $\nu/|\mathbf{b}|$ is small enough, or equivalently, the Péclet number is large) on the right vertical side of the computational domain.

We decompose the computational domain in two overlapping subdomains $\Omega_1 = (0, x_g + \delta_{12}/2) \times (-1,1)$ and $\Omega_2 = (x_g - \delta_{12}/2, 1) \times (-1,1)$ (where both x_g and δ_{12} will be precised later) and we solve the heterogeneous minimization problem (26) by the ICDD method (29)–(30). In agreement with names given in Sect. 5 for the homogeneous elliptic problem, the ICDD method (29)–(30) is named JGD, since the observation is on the interface and the controls are of Dirichlet type.

The boundary conditions are specified for the two subproblems as follows. For what concerns the hyperbolic problem, the inflow part of the external boundary is $(\partial\Omega_1 \setminus \Gamma)^{in} = \{(x,y) : x = -1,\ y > 0\}$ and there we set $\phi_D = 1$, while for the elliptic problem we set homogeneous Dirichlet condition $\phi_D = 0$ on the right vertical side and homogeneous Neumann condition $\nu \partial u/\partial n = 0$ on the two horizontal sides of $\partial\Omega_2 \setminus \Gamma_2$.

By taking some values of ν in the interval $[10^{-5}, 10^{-2}]$, we choose x_g and δ_{12} as shown in Table VIII.

The numerical solutions computed by hp-FEM of $\mathbb{Q}_p$ type are shown in Fig. 11, for $\nu = 10^{-2}$ and $\nu = 10^{-5}$. In the hyperbolic domain and along the y direction inside the elliptic domain the polynomial degree is $p = 5$, while along the x direction in the elliptic domain it is larger in order to capture the layer without oscillations (more precisely, it is $p = 8$ when $\nu = 10^{-2}$, $p = 12$ when $\nu = 10^{-3}$, $p = 16$ when $\nu = 10^{-4}$, $p = 20$ when $\nu = 10^{-5}$). As a matter of fact, for the solution of this problem GLS stabilizations either do not dump oscillations or show over diffusion.

In Table IX we report the number of iterations that JGD requires to converge up to the tolerance $\epsilon = 10^{-12}$.

Table IX. *Test case #5*. JGD iterations

δ_{12}	ν 10^{-2}	10^{-3}	10^{-4}	10^{-5}	δ_{12}	ν 10^{-2}	10^{-3}	10^{-4}	10^{-5}
$2 \cdot 10^{-5}$	21	22	16	11	$1 \cdot 10^{-3}$	14	13	6	2
$4 \cdot 10^{-5}$	17	20	14	9	$2 \cdot 10^{-3}$	13	11	4	2
$1 \cdot 10^{-4}$	19	17	13	6	$4 \cdot 10^{-3}$	12	7	3	–
$2 \cdot 10^{-4}$	17	16	11	4	$1 \cdot 10^{-2}$	10	6	2	–
$4 \cdot 10^{-4}$	17	14	9	3	$2 \cdot 10^{-2}$	8	4	2	–

We notice that the method is robust when the viscosity becomes very small w.r.t. the magnitude of the advective field. As for the homogeneous elliptic case, the number of iterations grows when the overlap thickness decreases, but it remains bounded when the viscosity tends to zero.

6.2. Test case #6

Let us consider problem (2) in $\Omega = (0,1)^2$, where ν is a small positive constant, $\mathbf{b} = [1,1]^t$, $\gamma = 1$, $f = 1$ and $\phi_D = 0$.

When ν is small enough, two boundary layers occur at the top and at the right sides of the computational domain. We analyze the behavior of ICDD method JGD when the elliptic coefficient ν ranges from 10^{-6} to 10^{-2}.

For any value of ν considered, we solve the global homogeneous elliptic problem (2) by (14) as well as the heterogeneous A – AD coupling (26) by ICDD method (29)– (30) (or equivalently (32)) by setting $\nu = 0$ in the subregion of the domain far from the layers.

We measure the difference in L^2-norm between the state solution of the homogeneous ICDD (with elliptic problems in all the subdomains) and that of the heterogeneous ICDD, as well as the efficiency of the ICDD method in terms of iterations count.

We split the computational domain in 2×2 rectangular subdomains whose interfaces are close to the boundary layers (see Fig. 12). We set $\Omega_1 = (0, x_\Gamma + \delta/2) \times (0, y_\Gamma + \delta/2)$, $\Omega_2 = (0, x_\Gamma + \delta/2) \times (y_\Gamma - \delta/2, 1)$, $\Omega_3 = (x_\Gamma - \delta/2, 1) \times (0, y_\Gamma + \delta/2)$ and $\Omega_4 = (x_\Gamma - \delta/2, 1) \times (y_\Gamma - \delta/2, 1)$, the thickness of the overlap is $\delta = 0.01$ (corresponding to 1% of the side of the computational domain) for all the cases, while $x_\Gamma = y_\Gamma$ will be specified later and they will be chosen so that they do not fall in the boundary layer region.

In the heterogeneous case, we solve the hyperbolic equation in the subdomain Ω_1 and the elliptic equation in Ω_k with $k = 2, 3, 4$. We set $\widetilde{\Omega}_2 = \cup_{k=2}^4 \Omega_k$.

In each subdomain we discretize the boundary value problems by $\mathbb{Q}_2$ Finite Elements, stabilized with Galerkin Least Squares (GLS) techniques (see [30]) for the elliptic case.

In Fig. 12 (right) we report the numerical solution for $\nu = 10^{-6}$, while in Table X we show the number of Bi-CGstab iterations required by JGD up to reducing the residual of 12 orders of magnitude for both homogeneous ($\#it_e$) and heterogeneous ($\#it_h$) couplings.

By denoting with u_e and u_h the state solutions of the homogeneous and heterogeneous couplings, respectively, we report the errors $\|u_e - u_h\|_{L^2(\Omega_1)}$ and $\|u_e - u_h\|_{L^2(\widetilde{\Omega}_2)}$.

Numerical results show that, for any considered value of ν, to solve the heterogeneous problem instead of the homogeneous one is advantageous and the differences between the heterogeneous and homogeneous solutions vanish when ν tends to zero.

The mesh in Ω_1 is fixed in 10×10 elements, while in the other subdomains we consider different meshes versus the values of ν. More precisely, we fix $50 \times n_\nu$ elements in Ω_2, $n_\nu \times 50$ in Ω_3 and $n_\nu \times n_\nu$ in Ω_4, with $n_\nu = 5$ when $\nu = 10^{-2},\ 10^{-3}, 10^{-4}$ and $n_\nu = 10$ when $\nu = 10^{-5},\ 10^{-6}$.

In all cases the meshes are non-matching on the overlaps.

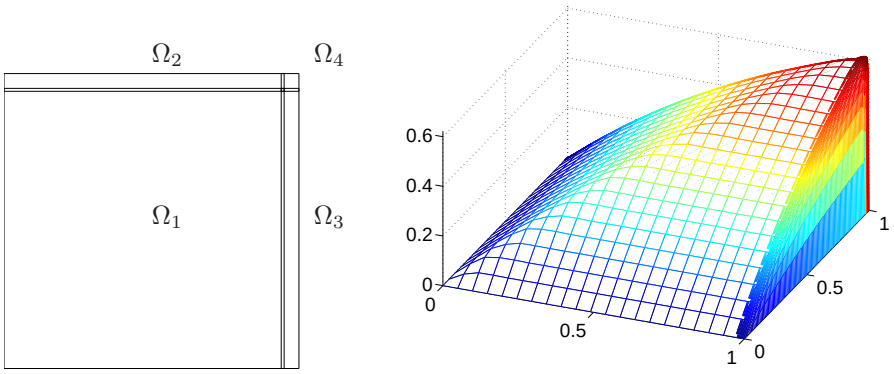

Figure 12. *Test case #6.* The decomposition of the computational domain (at left). The numerical solution of the heterogeneous coupling with $\nu = 10^{-6}$, obtained by stabilized $\mathbb{Q}_2$ finite elements (at right)

Table X. Test case #6. Iterations count and errors between heterogeneous solution u_h and global elliptic solution u_e

ν	x_Γ	$\#it_h$	$\#it_e$	$\|u_e - u_h\|_{L^2(\Omega_1)}$	$\|u_e - u_h\|_{L^2(\tilde{\Omega}_2)}$
10^{-2}	0.9	6	9	$9.48 \cdot 10^{-5}$	$1.61 \cdot 10^{-5}$
10^{-3}	0.95	5	11	$2.38 \cdot 10^{-6}$	$2.41 \cdot 10^{-7}$
10^{-4}	0.95	7	13	$1.83 \cdot 10^{-7}$	$1.10 \cdot 10^{-8}$
10^{-5}	0.95	7	13	$1.49 \cdot 10^{-7}$	$7.10 \cdot 10^{-9}$
10^{-6}	0.98	6	13	$1.48 \cdot 10^{-7}$	$6.90 \cdot 10^{-9}$

6.3. Test case #7

In this last test case we set $\Omega = (0, 0.5) \times (0, 1)$, $\nu = const > 0$ (it will be specified later), $\mathbf{b} = [1, \cos(2\pi x)]^t$, $\gamma = 0.1$, $f = 0$, and the following Dirichlet conditions:

$$\phi_D = \begin{cases} 10y(y - 0.3)(0.9 - y) & \text{when } x = 0 \\ 0 & \text{otherwise.} \end{cases}$$

When ν is small with respect to $|\mathbf{b}|$ two boundary layers occur on both right vertical and top horizontal side, while the solution is quite regular in the rest of the domain. Then we decompose the computational domain in 4 overlapping subdomains as shown in Fig. 13 (left) and we solve elliptic problems in both Ω_2 and Ω_3, and hyperbolic problems in Ω_1 and Ω_4. The interfaces are positioned in $x_g = 0.48 \pm \delta_{12}$ and $y_g = 0.87 \pm \delta_{13}$, the overlap thickness will be precised in Table XI.

The numerical solution of the heterogeneous coupling, computed for $\nu = 10^{-4}$, is shown in Fig. 13 (right). We have considered non-uniform discretization in Ω, more precisely, the mesh is finer in both Ω_2 and Ω_3, while it is coarser in Ω_1 and Ω_4, and they do not match on the overlaps. In all subdomains we discretize by $\mathbb{Q}_p$-FEM and we use different polynomial degree p and different mesh size h not only among subdomains, but also along x and y directions, in order to better fit the behaviour of the solution near the layers and to save up either CPU and memory elsewhere. In detail we use the following discretization (instead of showing the mesh size h, we write the number of elements ne along any direction, the subscript denotes the axis, either x or y):

domain	p_x	ne_x	p_y	ne_y
Ω_1	6	6	6	6
Ω_2	10	8	10	6
Ω_3	16	4	12	4
Ω_4	4	2	4	2

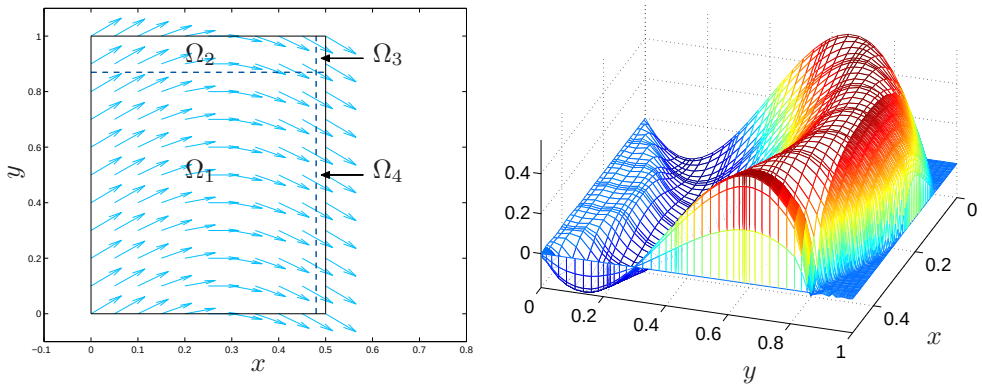

Figure 13. *Test case #7*. The computational domain and the advective field $\mathbf{b}$ (at left). The numerical solution of the heterogeneous coupling for $\nu = 10^{-4}$ with interfaces in $x_g = 0.48 \pm 5 \cdot 10^{-5}$ and $y_g = 0.87 \pm 10^{-4}$ (at right)

Table XI. *Test case #7*. JGD iterations when $\nu = 10^{-4}$. In all cases, $\delta_{13} = 2\delta_{12}$

δ_{12}	JGD iterations
$5 \cdot 10^{-5}$	21
$1 \cdot 10^{-4}$	17
$2.5 \cdot 10^{-4}$	12
$5 \cdot 10^{-4}$	10
$1 \cdot 10^{-3}$	8
$2.5 \cdot 10^{-3}$	7
$5 \cdot 10^{-3}$	6

As in the previous test cases the number of JGD iterations mildly depend on the overlap tichkness as it is shwon in Table XI.

ACKNOWLEDGEMENT

The first author acknowledges funding from the European Union Seventh Framework Programme (FP7/2007-2013) under grant agreement n° 294229.

REFERENCES

1. B. Smith, P. Bjørstad, and W. Gropp, *Domain Decomposition. Parallel Multilevel Methods for Elliptic Partial Differential Equations*. Cambridge: Cambridge University Press, 1996.
2. A. Quarteroni and A. Valli, *Domain Decomposition Methods for Partial Differential Equations*. Oxford Science Publications, 1999.
3. A. Toselli and O. Widlund, *Domain decomposition methods—algorithms and theory*, vol. 34 of *Springer Series in Computational Mathematics*. Berlin: Springer-Verlag, 2005.
4. R. Glowinski, Q. Dinh, and J. Periaux, "Domain decomposition methods for nonlinear problems in fluid dynamics," *Comput. Methods Appl. Mech. Engrg.*, vol. 40, no. 1, pp. 27–109, 1983.
5. J.-L. Lions and O. Pironneau, "Algorithmes parallèles pour la solution de problèmes aux limites," *C. R. Acad. Sci. Paris Sér. I Math.*, vol. t. 327, pp. 947–952, 1998.
6. M. Discacciati, P. Gervasio, and A. Quarteroni, *Heterogeneous mathematical models in fluid dynamics and associated solution algorithms*, vol. 2040 of *Lecture Notes in Mathematics*, ch. 2, pp. 57–123. Springer, 2011. Lectures given at the C.I.M.E. Summer School held in Cetraro, July 2009. Edited by G. Naldi and G. Russo.
7. P. Gervasio, J.-L. Lions, and A. Quarteroni, "Heterogeneous coupling by virtual control methods," *Numerische Mathematik*, vol. 90, no. 2, pp. 241–264, 2001.
8. E. Miglio, A. Quarteroni, and F. Saleri, "Coupling of free surface and groundwater flows," *Computers & fluids*, vol. 32, pp. 73–83, 2003.

9. M. Discacciati, E. Miglio, and A. Quarteroni, "Mathematical and Numerical Models for Coupling Surface and Groundwater Flows," *Appl. Numer. Math.*, vol. 43, no. 1-2, pp. 57–74, 2002. 19th Dundee Biennial Conference on Numerical Analysis (2001).
10. M. Discacciati, P. Gervasio, and A. Quarteroni, "The Interface Control Domain Decomposition (ICDD) Method for Elliptic Problems," tech. rep., MOX, Politecnico di Milano, 2012. Submitted to SIAM J. on Control and Optimization.
11. P. Grisvard, *Elliptic Problems in Nonsmooth Domains*. Boston, MA: Pitman (Advanced Publishing Program), 1985.
12. R. Adams and J. Fournier, *Sobolev spaces*, vol. 140 of *Pure and Applied Mathematics (Amsterdam)*. Elsevier/Academic Press, Amsterdam, second ed., 2003.
13. A. Quarteroni and A. Valli, *Numerical Approximation of Partial Differential Equations*. Heidelberg: Springer Verlag, 1994.
14. J.-L. Lions, *Optimal Control of Systems Governed by Partial Differential Equations*. New York: Springer-Verlag, 1971.
15. M. Discacciati, P. Gervasio, and A. Quarteroni, "Interface Control Domain Decomposition Methods: numerical aspects and validation," tech. rep., MOX - Politecnico di Milano, 2013. In preparation.
16. V. Agoshkov, P. Gervasio, and A. Quarteroni, "Optimal control in heterogeneous domain decomposition methods for advection-diffusion equations," *Mediterr. J. Math.*, vol. 3, no. 2, pp. 147–176, 2006.
17. F. Gastaldi, A. Quarteroni, and G. S. Landriani, "On the coupling of two dimensional hyperbolic and elliptic equations: analytical and numerical approach," in *Third International Symposium on Domain Decomposition Methods for Partial Differential Equations* (J. T.F.Chan, R.Glowinski and O.B.Widlund, eds.), (Philadelphia), pp. 22–63, SIAM, 1990.
18. P. Blanco, P. Gervasio, and A. Quarteroni, "Extended variational formulation for heterogeneous partial differential equations," *Comput. Methods in Applied Math.*, vol. 11, no. 2, pp. 141–172, 2011.
19. F. Gastaldi and A. Quarteroni, "On the coupling of hyperbolic and parabolic systems: analytical and numerical approach.," *Appl. Numer. Math.*, vol. 6, no. 1, pp. 3–31, 1989.
20. L. Marini and A. Quarteroni, "A relaxation procedure for domain decomposition methods using finite elements," *Numer.Math.*, vol. 55, pp. 575–598, 1989.
21. P. Blanco, P. Gervasio, and A. Quarteroni, "Mortar coupling for heterogeneous partial differential equations," in *Domain Decomposition Methods in Science and Engineering XX (DD20, San Diego 2011)* (R. Bank, M. Holst, O. Widlund, and J. Xu, eds.), (Berlin), Springer Verlag, 2013.
22. C. Canuto, M. Y. Hussaini, A. Quarteroni, and T. A. Zang, *Spectral Methods. Fundamentals in Single Domains* . Heidelberg: Springer, 2006.
23. C. Canuto, M. Y. Hussaini, A. Quarteroni, and T. A. Zang, *Spectral Methods. Evolution to Complex Geometries and Applications to Fluid Dynamics*. Heidelberg: Springer, 2007.
24. C. Canuto, P. Gervasio, and A. Quarteroni, "Finite-Element Preconditioning of G-NI Spectral Methods," *SIAM J. Sci. Comput.*, vol. 31, no. 6, pp. 4422–4451, 2009/10.
25. H. van der Vorst, *Iterative Krylov methods for large linear systems*, vol. 13 of *Cambridge Monographs on Applied and Computational Mathematics*. Cambridge: Cambridge University Press, 2003.
26. T. Rees, H. Dollar, and A. Wathen, "Optimal solvers for PDE-constrained optimization," *SIAM J. Sci. Comput.*, vol. 32, no. 1, pp. 271–298, 2010.
27. H. Dollar, N. Gould, M. Stoll, and A. Wathen, "Preconditioning saddle-point systems with applications in optimization," *SIAM J. Sci. Comput.*, vol. 32, no. 1, pp. 249–270, 2010.
28. A. Borzì and V. Schulz, "Multigrid methods for PDE optimization," *SIAM Rev.*, vol. 51, no. 2, pp. 361–395, 2009.
29. M. Benzi, E. Haber, and L. Taralli, "A preconditioning technique for a class of pde-constrained optimization problems," *Advances in Computational Mathematics*, vol. 35, pp. 149–173, 2011.
30. L. Franca, S. Frey, and T. Hughes, "Stabilized finite element methods: I. Application to the Advective-Diffusive model," *Comput. Meth. Appl. Mech. Engrg.*, vol. 95, pp. 253–276, 1992.
31. P. Gervasio, *Risoluzione di equazioni alle derivate parziali con metodi spettrali in regioni partizionate in sottodomini*. PhD thesis, Università degli Studi di Milano, 1995.
32. A. Quarteroni, *Numerical Models for Differential Problems*. Series MS&A, Vol. 2, Milano: Springer, 2009.

Recent publications :

MATHEMATICS INSTITUTE OF COMPUTATIONAL SCIENCE AND ENGINEERING
Section of Mathematics
Ecole Polytechnique Fédérale
CH-1015 Lausanne

48.2012 G. MIGLORATI, F. NOBILE, E. VON SCHWERIN, R. TEMPONE:
Approximation of quantities of interest in stochastic PDES by the random discrete L^2 projection on polynomial spaces

01.2013 A. ABDULLE, A. BLUMENTHAL:
Stabilized multilevel Monte Carlo method for stiff stochastic differential equations

02.2013 D. N. ARNOLD, D. BOFFI, F. BONIZZONI:
Tensor product finite element differential forms and their approximation properties

03.2013 N. GUGLIELMI, D. KRESSNER, C. LUBICH:
Low-rank differential equations for Hamiltonian matrix nearness problems

04.2013 P. CHEN, A. QUARTERONI, G. ROZZA:
A weighted reduced basis method for elliptic partial differential equations with random input data

05.2013 P. CHEN, A. QUARTERONI, G. ROZZA:
A weighted empirical interpolation method: a priori convergence analysis and applications

06.2013 R. SCHNEIDER, A. USCHMAJEW:
Approximation rates for the hierarchical tensor format in periodic Sobolev spaces

07.2013 C. BAYER, H. HOEL, E. VON SCHWERIN, R. TEMPONE:
On non-asymptotic optimal stopping criteria in Monte Carlo simulation.

08.2013 L. GRASEDYCK, D. KRESSNER, C. TOBLER:
A literature survey of low-rank tensor approximation techniques

09.2013 M. KAROW, D. KRESSNER:
On a perturbation bound for invariant subspaces of matrices

10.2013 A. ABDULLE:
Numerical homogenization methods

11.2013 PH. BLANC:
Lower bound for the maximum of some derivative of Hardy's function

12.2013 A. ABDULLE, Y. BAI, G. VILMART:
Reduced basis finite element heterogeneous multiscale method for quasilinear elliptic homogenization problems

13.2013 P. CHEN, A. QUARTERONI:
Accurate and efficient evaluation of failure probability for partial different equations with random input data

14.2013 M. DISCACCIATI, P. GERVASIO, A. QUARTERONI:
Interface control domain decomposition (ICDD) methods for coupled diffusion and advection-diffusion problems